UNIVERSIDADE DE BRASÍLIA

FACULDADE DE TECNOLOGIA

DEPARTAMENTO DE ENGENHARIA CIVIL E AMBIENTAL

AVALIAÇÃO DA INSTABILIDADE EM REJEITOS DE MINÉRIO DE FERRO: INFLUÊNCIA DA GRANULOMETRIA E DA TRAJETÓRIA DE TENSÕES

ROBERTO AGUIAR DOS SANTOS

ORIENTADORA: MICHÉLE DAL TOÉ CASAGRANDE, DSc.

COORIENTADOR: ANDY FOURIE, PhD.

TESE DE DOUTORADO EM GEOTECNIA

PUBLICAÇÃO: G.TD-205/2025

BRASÍLIA / DF: 29 JULHO / 2025

UNIVERSIDADE DE BRASÍLIA

FACULDADE DE TECNOLOGIA

DEPARTAMENTO DE ENGENHARIA CIVIL E AMBIENTAL

EXPERIMENTAL ASSESSMENT OF THE INSTABILITY LOCUS IN IRON ORE TAILINGS: INFLUENCE OF GRADING AND STRESS PATHS

ROBERTO AGUIAR DOS SANTOS

SUPERVISOR: MICHÉLE DAL TOÉ CASAGRANDE, DSc.

CO-SUPERVISOR: ANDY FOURIE, PhD.

TESE DE DOUTORADO EM GEOTECNIA

PUBLICAÇÃO: G.TD-205/2025

BRASÍLIA / DF: 29 JULHO / 2025

UNIVERSIDADE DE BRASÍLIA
FACULDADE DE TECNOLOGIA
DEPARTAMENTO DE ENGENHARIA CIVIL E AMBIENTAL

EXPERIMENTAL ASSESSMENT OF THE INSTABILITY LOCUS IN IRON ORE TAILINGS: INFLUENCE OF GRADING AND STRESS PATHS

ROBERTO AGUIAR DOS SANTOS

TESE DE DOUTORADO SUBMETIDA AO DEPARTAMENTO DE ENGENHARIA CIVIL E AMBIENTAL DA UNIVERSIDADE DE BRASÍLIA COMO PARTE DOS REQUISITOS NECESSÁRIOS PARA A OBTENÇÃO DO GRAU DE DOUTOR.

APROVADA POR:

_____
MICHÉLE DAL TOÉ CASAGRANDE, DSc.
(Universidade de Brasília)
(ORIENTADOR)

_____
ANDRÉ PACHECO ASSIS, PhD
(Universidade de Brasília)
(EXAMINADOR INTERNO)

_____
PAULO COELHO, PhD
(Universidade de Coimbra)
(EXAMINADOR EXTERNO)

_____
FELIPE DE MORAES RUSSO, DSc.
(VALE)
(EXAMINADOR EXTERNO)

BRASÍLIA/DF, 29 de JULHO de 2025

FICHA CATALOGRÁFICA

DOS SANTOS, ROBERTO AGUIAR
Experimental Assessment of the Instability Locus in Iron Ore Tailings: Influence of Grading and Stress Paths
(Distrito Federal) 2025.
xv, - 67 p., 210 x 297 mm (ENC/FT/UnB, Doutor, Geotecnia, 2025)
Tese de Doutorado - Universidade de Brasília. Faculdade de Tecnologia.
Departamento de Engenharia Civil e Ambiental.
1. Rejeitos de minério de ferro 2. Mecânica dos solos nos estados críticos
3. Liquefação 4. Hollow cylinder test
I. ENC/FT/UnB II. Doutor

REFERÊNCIA BIBLIOGRÁFICA

DOS SANTOS, R. A. (2025 Experimental Assessment of the Instability Locus in Iron Ore Tailings: Influence of Grading and Stress Paths, Tese de Doutorado, Publicação G.TD-205/2025, Departamento de Engenharia Civil e Ambiental, Universidade de Brasília, Brasília, DF, 67p.

CESSÃO DE DIREITOS

NOME DO AUTOR: Roberto Aguiar dos Santos
TÍTULO DA TESE DE DOUTORADO: Experimental Assessment of the Instability Locus in Iron Ore Tailings: Influence of Grading and Stress Paths.
GRAU / ANO: Doutor /2025.

Roberto Aguiar dos Santos
Universidade de Brasília, Secretaria de Coordenação de Pós-Graduação em Geotecnia
Campus Darcy Ribeiro, Departamento de Engenharia Civil e Ambiental, Prédio SG-12,
Universidade de Brasília. CEP: 70910-900 – Brasília, DF – Brasil

AGRADECIMENTOS

A Deus, por sempre ser generoso e bondoso comigo.

À minha querida amada, Tálita Nola, que sempre me incentivou a alcançar meus objetivos. Seu apoio e encorajamento nas dificuldades foram fundamentais.

À minha filha, Laura. Seu sorriso foi um dos motores que me impulsionaram nos momentos finais desta tese.

Aos meus pais e irmãos, que sempre acreditaram em mim e torceram pelo meu sucesso. O apoio de vocês foi essencial ao longo da minha trajetória.

Aos meus sogros, cunhado e cunhada, pelo carinho e apoio.

À minha orientadora, Michéle Casagrande. Obrigado por toda a orientação, amizade e ensinamentos ao longo desta tese.

Ao meu coorientador, Andy Fourie. Sua paciência, generosidade e humildade são admiráveis. Obrigado por aceitar fazer parte desta pesquisa.

À Cristina Vulpe. Agradeço por todo o apoio e amizade durante o período em que estive na UWA. Seu suporte diário foi fundamental para a conclusão bem-sucedida do extenso programa experimental desta tese.

À amiga Ana Claudia Telles. Obrigado por todo o suporte e pelo treinamento na operação do *hollow cylinder*. Nossas discussões técnicas sobre o comportamento de rejeitos foram fantásticas. Você e o Antônio sempre foram muito generosos comigo e com a Tálita.

Ao David Reid. Agradeço pelo treinamento com a técnica de air-dried. Você me mostrou que, por trás de um profissional de destaque internacional, há incontáveis horas de trabalho exaustivo no laboratório.

Aos demais amigos da UWA – Alexandra Halliday, Bandana, Congyang Yu, Erwin, Felipe Urbina, Nilan Jayasiri, Riccardo Fanni, Temogo Marble, e Vijay – meu muito obrigado!

Ao Mike Jefferies. Muito obrigado por toda sua generosidade e ensinamentos.

Aos colegas do Laboratório de Geotecnia da Vale, deixo registrado meu sincero agradecimento a todos que, de alguma forma, contribuíram para a realização desta pesquisa. Meu agradecimento especial ao Inácio Carvalho. Seu apoio foi crucial para o desenvolvimento deste trabalho. Sem ele, não teria sido possível enviar 700 kg de rejeito de minério de ferro do Brasil para a Austrália. Agradeço também aos amigos João Paulo, Àtila Rochido, Pedro Cacciari e Rosiane Soares, por acreditarem nesta pesquisa e oferecerem suporte essencial ao longo de sua execução.

Por fim, agradeço ao CNPq pela concessão da bolsa de doutorado sanduíche, por meio do processo nº 200173/2022-7.

RESUMO

Garantir a estabilidade de barragens de rejeitos (TSFs) continua sendo um dos principais desafios da indústria da mineração. A liquefação estática tem sido identificada como um dos principais mecanismos por trás das recentes falhas em barragens de rejeitos. Quando a trajetória de tensões *in situ* atinge ou excede a resistência não drenada do solo, uma perturbação mínima sob condições não drenadas pode desencadear a liquefação, potencialmente levando a uma ruptura por fluxo. Esse processo resulta em perda abrupta de resistência, rápida acumulação de deformações e elevada poro pressão. O limite de resistência não drenada no qual esse processo se inicia é conhecido como linha de instabilidade, tipicamente representada em termos de tensões efetivas no plano q–p′. Apesar dos avanços nas técnicas laboratoriais, a ausência de sinais prévios às falhas recentes por liquefação evidencia lacunas importantes na compreensão dos fatores que governam a instabilidade em rejeitos. Este estudo investiga os fatores que afetam a linha de instabilidade em rejeitos de minério de ferro, com foco na influência da distribuição granulométrica e de trajetória de tensões complexas. Além disso, avalia-se a aplicabilidade de medições de velocidade de onda de cisalhamento (V_s) para fins de monitoramento e o papel do parâmetro de estado em Vs. Um programa abrangente de ensaios laboratoriais foi conduzido, incluindo ensaios triaxiais, ensaios em *hollow cylinder*, *bender elements* e de coluna ressonante. Os resultados experimentais mostraram que tanto a linha de estado crítico (nos planos e–p′ e q–p′) quanto a razão de tensões na instabilidade são afetadas pelo teor de finos. Esse comportamento pode ser atribuído a alterações na mineralogia e na forma das partículas introduzidas pela adição de finos nas misturas estudadas. Ensaios no *hollow cylinder* foram utilizados para simular condições de deformação plana, típicas de estados de tensões abaixo de taludes. Esses ensaios indicaram que o aumento tanto na rotação dos esforços principais (α) quanto na razão de tensões principais intermediária (b) resulta em uma resposta não drenada mais contrátil em comparação ao cisalhamento triaxial convencional, levando a menores razões de tensões na instabilidade. A magnitude desse efeito mostrou-se dependente do parâmetro de estado inicial (ψ_0). Os ensaios com *bender elements* realizados durante o caminho de tensões do tipo CSD demonstraram que a V_s é um indicador confiável das variações da tensão efetiva média em rejeitos. Além disso, os resultados indicam que em estados densos, as medições de V_s apresentam menor dependência da tensão quando comparadas a estados soltos. As conclusões deste trabalho oferecem subsídios relevantes sobre os principais fatores que controlam a instabilidade em rejeitos de minério de ferro e

fornecem evidências experimentais que podem contribuir para uma gestão mais segura e eficiente de barragens de rejeitos.

ABSTRACT

Ensuring the stability of tailings storage facilities (TSFs) remains one of the major challenges in the mining industry. Static liquefaction has been identified as one of the main mechanisms behind recent tailings dam failures. When the in-situ stress path reaches or exceeds the current undrained strength of the soil, a minor perturbation under undrained conditions may trigger liquefaction, potentially leading to flow failure. This process results in an abrupt loss of strength, rapid strain accumulation, and the generation of positive excess pore pressures. The undrained strength limit at which this onset occurs is referred to as the instability line, typically represented in terms of effective stress in the q-p′ plane. Despite advances in laboratory techniques, the lack of warning preceding recent liquefaction failures highlights important gaps in understanding the factors that govern instability in tailings. This study investigates factors affecting the instability line in iron ore tailings, with a focus on the influence of material grading and complex stress paths. Additionally, it assesses the applicability of shear wave velocity measurements for monitoring purposes and examines the role of the state parameter in controlling shear wave velocity behaviour. A comprehensive laboratory testing programme was conducted, including triaxial compression tests, hollow cylinder tests, bender element tests, and resonant column tests. The experimental results demonstrated that both the critical state line (in the e-p′ and q-p′ planes) and the instability stress ratio are affected by fines content. This behaviour may be attributed to changes in mineralogy and particle shape introduced by the addition of fines in the studied mixtures. Hollow cylinder tests were used to simulate plane strain conditions, which are typical of below-slope stress states. These tests showed that increases in both principal stress rotation (α) and intermediate principal stress ratio (b) lead to a more contractive undrained response compared to standard triaxial compression, resulting in lower instability stress ratios. The magnitude of this effect was found to depend on the initial state parameter (ψ_0). Bender element tests performed during the CSD stress path demonstrated that shear wave velocity (V_s) is a reliable indicator of changes in mean effective stress in tailings. Furthermore, the results indicate that V_s measurements in dense states exhibit lower stress dependency compared to loose states. The findings provide insights into key factors controlling instability in iron ore tailings and offer experimental evidence that may contribute to the safer and more efficient management of tailings storage facilities.

TABLE OF CONTENTS

LIST OF FIGURES

LIST OF TABLES

NOTATION LIST

AD	Air dried
ANI	Ambient noise interferometry
b	Intermediate principal stress ratio
B	Skempton's pore pressure coefficient
c	Consolidated
cs	Critical state
CSD	Constant shear drained
CSL	Critical state line
CSSM	Critical state soil mechanics
D_{50}	Median particle size
e	Void ratio
e_{cs}	Critical state void ratio
e_r, λ, ζ	Parameters of the CSL power-law equation
FC	Fine content
GISTM	Global Industry Standard on Tailings Management
G_{max}	Shear modulus
G_{ref}	Small-strain shear modulus
G_s	Specific gravity
HCTS	Hollow cylinder torsional shear test
IL	Instability
IOT	Iron ore tailings
K_c	Anisotropic consolidation ratio
LE	Lateral extrusion
MT	Moist tamping
M_{tc}	Critical friction ratio, equals η_c at the critical state.
p'	Mean effective stress
p_c'	Mean effective stress at consolidation
p_{ref}	Mean effective stress at reference pressure of 100 kPa
q	Triaxial deviatoric stress $q = \sigma_1 - \sigma_3$
q_{13}	
RCT	Resonant column test
SEM	Scanning electron microscopy
TSF	Tailings storage facility
TX-C	Triaxial compression

UWA	The University of Western Australia
V_s	Seismic shear wave velocity
V_{s1}	Normalised shear wave velocity
α	direction of major principal stress relative to the vertical axis or
β	Fitting exponent
ε_v	Volumetric strain
ε_v	Volumetric strain
ε_q	Deviatoric strains
ε_a	Axial strain
η_{IL}	Stress ratio at onset instability
η	Stress ratio
σ_1	Major principal stress
σ_2	Intermediate principal stress
σ_3	Minor principal stress
ψ_0	State parameter, $\psi_0 = e - e_{cs}$
Γ, λ_e	Semi-log critical state line parameters: intercept at 1 kPa and slope

CHAPTER 1

1. INTRODUCTION

1.1. BACKGROUND

In recent decades, numerous Tailings Storage Facilities (TSFs) failures have occurred, including Stava (Chandler & Tosatti, 1995; Morgenstern, 2001), Merriespruit (Fourie & Papageorgiou, 2001), Fundão (Morgenstern et al., 2016), Mount Polley (Morgenstern et al., 2015), Cadia (Jefferies et al., 2019), and Feijão (Robertson et al., 2019; Arroyo & Gens, 2021). These failures have resulted in loss of life and significant environmental impacts, with static liquefaction failure being identified as one of the main causes of this persistent issue in the mining industry (Riveros & Sadrekarimi, 2021).

1.2. MOTIVATION

In many of these recent cases, static liquefaction was identified as the main mode of failure (Riveros & Sadrekarimi, 2021). Static liquefaction triggering occurs when the in-situ stress path reaches the instability stress ratio ($\eta_{IL} = q/p'$). Some typical triggering mechanisms include displacement of the foundation or underlying layers, dam raising, or changes in pore pressure due to an increase in the water table (Martin & McRoberts, 1999; Morgenstern et al., 2016; Ledesma et al., 2022).

Given the high frequency of these events, several studies have been conducted to improve techniques for evaluating the susceptibility of materials to liquefaction and to better understand the mechanisms causing these failures (e.g., Carrera et al., 2011; Bedin et al., 2012; Fanni et al., 2022; Macedo & Vergarey, 2022). However, despite advancements in TSF design and monitoring, failures continue to occur, with catastrophic consequences.

Even though instability is recognized as a crucial factor in assessing tailings liquefaction, laboratory tests to evaluate instability is not yet routine (Jefferies et al., 2019). The effect of fines content, stress rotation and intermediate principal stress on the instability of mining tailings is not well studied. This thesis aims to address these gaps through experimental investigations of iron ore tailings.

1.3. RESEARCH OBJECTIVES

The objectives of this thesis are:

a) To investigate the influence of fines content on the instability and critical state locus;

b) To compare the behaviour of iron ore tailings under axisymmetric condition with that under below slope stress condition;

c) To assess the applicability of shear wave velocity for monitoring effective stress variations during CSD (Constant Shear Drained) stress path;

d) To evaluate the influence of the state parameter on shear wave velocity.

1.4. SCOPE OF STUDY

This study investigates the instability behaviour of iron ore tailings, with a focus on the influence of material gradation, stress path conditions, and shear wave velocity measurements. Even though this research provides valuable contributions regarding key factors that affect the instability of mining tailings, some limitations must be acknowledged to clearly define the scope of this thesis.

The main limitations are organized into three cores areas:

- *Grading effects*: The effect of fines content on the critical state line (CSL) is investigate using laboratory-reconstituted specimens with controlled gradation. Effects of specimen reconstitution method, in situ sampling and aging process were not addressed in this study.

- *Stress path effects*: Axisymmetric and non-axisymmetric loading paths are investigated, including below-slope stress conditions simulated using a hollow cylinder apparatus. However, the analysis is limited to monotonic loadings and performed in reconstituted specimens. The influence of in situ fabric and cyclic loading on mechanic response were not considered in this study.

- *Shear wave velocity measurements*: The potential of shear wave velocity as a tool for monitoring effective stress reduction during CSD stress path was evaluated. Furthermore, a boundary between contractive and dilative behaviour was also

proposed based on shear wave velocity measurements. Although these findings are developed from well-controlled laboratory conditions, the effect of fabric, anisotropy, creep, aging, and cementation remain outside the scope of this study.

The findings are based on experimental results from Brazilian iron ore tailings. Any extrapolation of these findings to field conditions or to other tailings materials should be made with caution.

1.5. STRUCTURE OF THE THESIS

This thesis is structured into five chapters, each contributing to the understanding of key factor influencing the instability behaviour of iron ore tailings:

- **Chapter 1 – Introduction**: Introduces the research background, motivation, research objectives, scope, and the overall structure of the thesis.
- **Chapter 2 – Literature review**: Provides an overview of relevant concepts and previous studies, including concepts from critical state soil mechanics, instability, the influence of grading on CSL, and the application of shear wave velocity measurements for tailings monitoring.
- **Chapter 3 – Materials and Experimental Programme**: Describes the process of preparation and characterization of the iron ore tailings mixtures. It also details the experimental procedures adopted in the triaxial compression tests, hollow cylinder tests, and bender elements and resonant column tests.
- **Chapter 4 – Results and Discussion**: Presents and analyses the experimental findings, focusing on the influence of grading and stress path conditions on the instability stress ratio. The behaviour of shear wave velocity (V_s) is also examined with respect to changes during CSD stress path and its relationship with the state parameter.
- **Chapter 5 – Conclusions and Recommendations:** Summarizes the main conclusions of the study and provides suggestions for future research.
- **Chapter 6 – Conclusions (in Portuguese):** Summarizes the main conclusions of the study in Portuguese.

CHAPTER 2

2. LITERATURE REVIEW

This chapter provides an overview of the literature on critical state soil mechanics, the role of instability stress ratio in liquefaction assessment and the use of shear wave velocity for monitoring tailings storage facilities. This review establishes the context for this thesis and highlights existing gaps in the literature.

2.1 CRITICAL STATE SOIL MECHANICS

Casagrande (1936) introduced the concept of critical state which establishes a relationship between specimen density, volume change and effective stress during shearing. When a soil specimen is sheared and is subjected to large strains, it reaches a constant volume and continues to deform without further changes in void ratio and effective stress. The void ratio achieved at this stage is referred to as the void ratio at the critical state. The critical state is not unique, as it depends on the effective stress at onset of shearing. The set of different void ratio and mean effective stress at the critical state defines the critical state locus (CSL) in the $e-p'$ plane. The concept of the critical state provided a conceptual basis for the development of the well-known Critical State Soil Mechanics (Schofield & Wroth, 1968).

Been & Jefferies (1985) proposed a parameter that combines the influence of void ratio and mean effective stress, known as state parameter (ψ_0). This parameter is defined as the void ratio difference between the void ratio at onset of shearing and the void ratio on the critical state, both obtained at the same mean effective stress (Figure 2.1). Dense soils have negative ψ_0 and exhibit dilative behaviour at large strain, whereas loose soils are contractive and have a positive ψ_0. The state parameter has been widely used to describe the behaviour of granular material across a broad range of densities and mean effective stress.

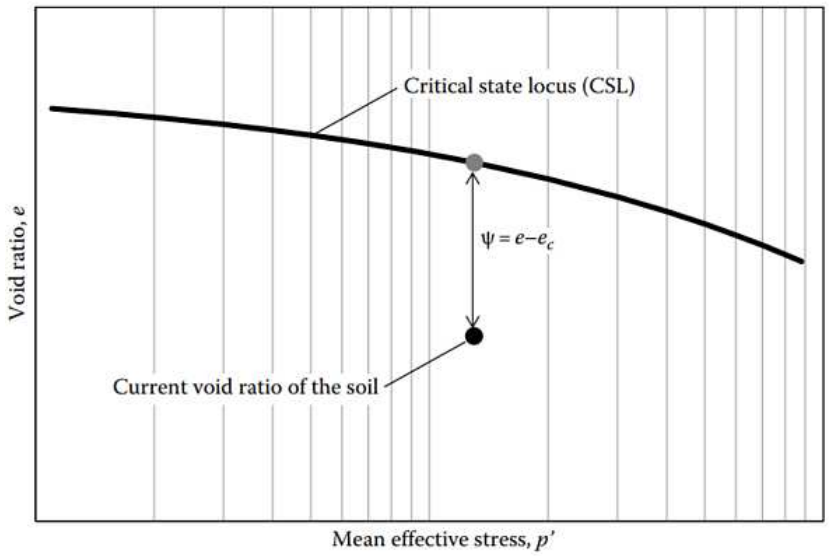

Figure 2.1. Definition of state parameter (Jefferies & Been, 2015).

Mine tailings derived from hard rock ore deposits may contain significant amount of fines content (more than 20% by mass) (Fourie et al., 2022). The influence of the fines content on the behaviour on tailings has received limited attention in the past (Wiklund, 2018; Silva et al., 2021). Been & Jefferies (1986) analysed the behaviour of the Kogyuk 350 sand with different fines contents. The authors observed that the slope of the CSL increases with increasing fines content. Furthermore, the triaxial tests carried out on these mixtures demonstrated that specimens with the same state parameter behaved similarly, even if they had different fines contents.

2.2. INSTABILITY

The term 'instability' is often used to refer to behaviour where large plastic strain is rapidly generated due to the inability of a soil element to support a given load (Wanatowski et al., 2010). Instability is closely linked to static liquefaction, as triggering occurs when the in-situ stress path reaches the instability stress ratio (η_{IL}). Stress ratio ($\eta = q/p'$) increases until it reaches η_{IL}, due to an increase in deviatoric stress or a decrease in mean effective stress caused by rising pore pressure (Jefferies and Been, 2015). When η exceeds η_{IL}, the subsequent behaviour depends on whether the adjacent soil can accommodate the load redistributed from the overloaded zone. If this is not possible, the progression to failure accelerates and this can result in almost instantaneous collapse of the soil mass (Jefferies et al., 2019).

Some typical triggering mechanisms include dam raising, changes in pore pressure due to an increase in the water table, displacement of the foundation or underlying layers

(Martin & McRoberts, 1999; Morgenstern et al., 2016). Although the undrained stress path is commonly used to conceptualise the triggering mechanism, field-scale failures can also occur under drained stress conditions (Fanni et al., 2022). Figure 2.2 schematically illustrates the undrained and drained stress paths that lead to the onset of instability in loose specimens. In an undrained stress path (red line), instability is triggered by an increase in pore water pressure. In contrast, in a drained stress path (green line), also referred to as constant shear drained (CSD) stress path (Anderson & Sitar, 1995), can lead to instability due to a reduction in mean effective stress while the deviatoric stress remains constant. Once instability is exceeded and drainage is inhibited, the soil transitions from drained to undrained behaviour (Jefferies et al., 2019).

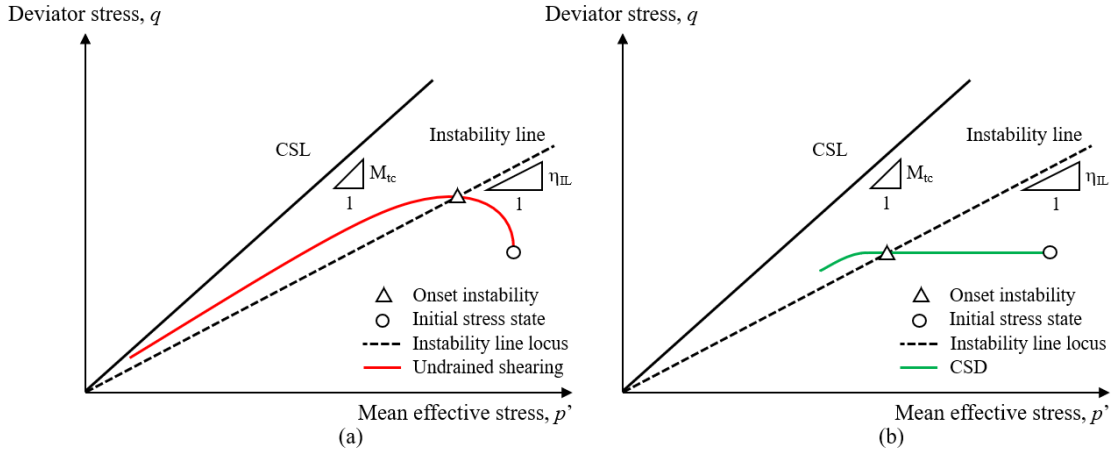

Figure 2.2. Schematic of instability locus in loose specimens leading to static liquefaction under: (a) undrained shearing; (b) constant shear drained (CSD) stress paths

Constant shear drained stress path has been recognized as the stress path that led to the static liquefaction triggering of various earthworks, such as Wachusett Dam (Olson et al., 2000), Stava (Morgenstern, 2001), and more recently Edenville–Sanford Dam (Babaki & Tannant, 2024). CSD represents a stress path that simulates soil behaviour on slopes under slowly rising-water tables (Lourenço et al., 2011).

Several studies have used laboratory tests to evaluate the static liquefaction triggering under the CSD stress path (e.g., Fanni et al., 2022; Fotovvat et al., 2024). Monitoring strains during the CSD stress path in laboratory tests has shown that the onset of instability occurs at very low strains, typically less than 0.5% (Wanatowski et al., 2010; Yang et al., 2022). Monitoring displacements associated with this level of strain using

existing monitoring technologies poses challenges for issuing precautionary alerts for flow failure of slopes in field conditions (Yang et al., 2022, Fourie et al., 2022).

Relationships between η_{IL} and ψ have been used to assess both drained and undrained triggering conditions (e.g. Chu et al., 2003; Reid, 2020). From triaxial compression (TC) tests performed on different sands and tailings materials, Reid (2020) compiled a database illustrating the influence of the ψ on η_{IL} (Figure 2.3). A general trend was observed, where η_{IL} increases as density increases (i.e. decreasing ψ). Analysis linking ψ on η_{IL} have played an important role in forensic investigations of recent TSF failures (e.g., Fundão - Morgenstern et al., 2016; Cadia - Jefferies et al., 2019).

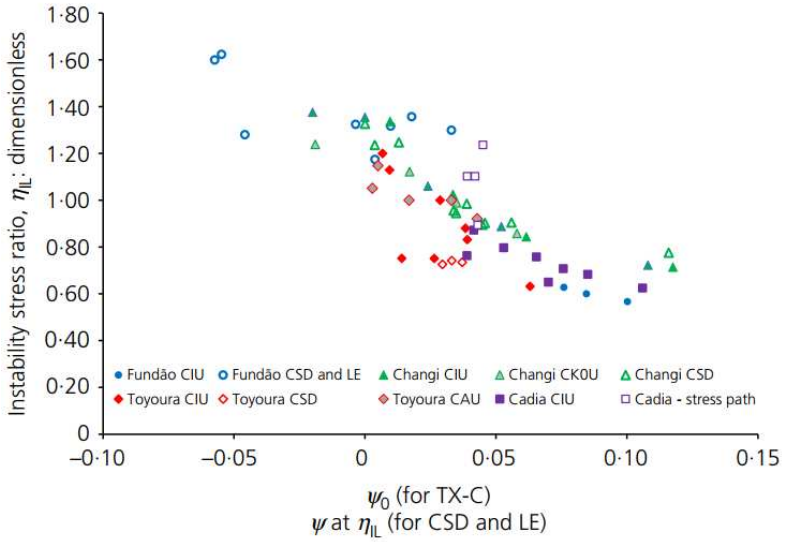

Figure 2.3. Instability stress ratios against state parameter for a range of soils and tailings (Reid, 2020).

Although there has been progress in producing data related to the onset of instability, the vast majority of these test studies have been performed on samples under axisymmetric conditions (Reid, 2020).

Despite recent scientific advances in the assessment of static liquefaction triggering, laboratory element testing techniques and numerical approaches for analysing the stress-strain behaviour of TSF perimeter embankments still require improvement (Reid et al., 2022a). The stress condition that exists below the embankment slope differ from those simulated in axisymmetric triaxial tests, as illustrated in Figure 2.4. This figure shows

two distinct stress conditions: below level ground (axisymmetric condition) and below slope (plane strain condition). The below level ground represents the stress condition far from the embankment slope, where the conventional triaxial test are widely used for simulation (i.e., $\sigma_2=\sigma_3$). In contrasts, in the below slope condition lateral strain is constrained, resulting in a plane strain where the intermediate and minor principal stresses are not equal ($\sigma_2\neq\sigma_3$). Besides, under the below slope condition the angle between the principal stress direction (α) is not null and tends to increases as it approaches the toe of the slope. The angle α represents the inclination of the major principal stress relative to the vertical direction.

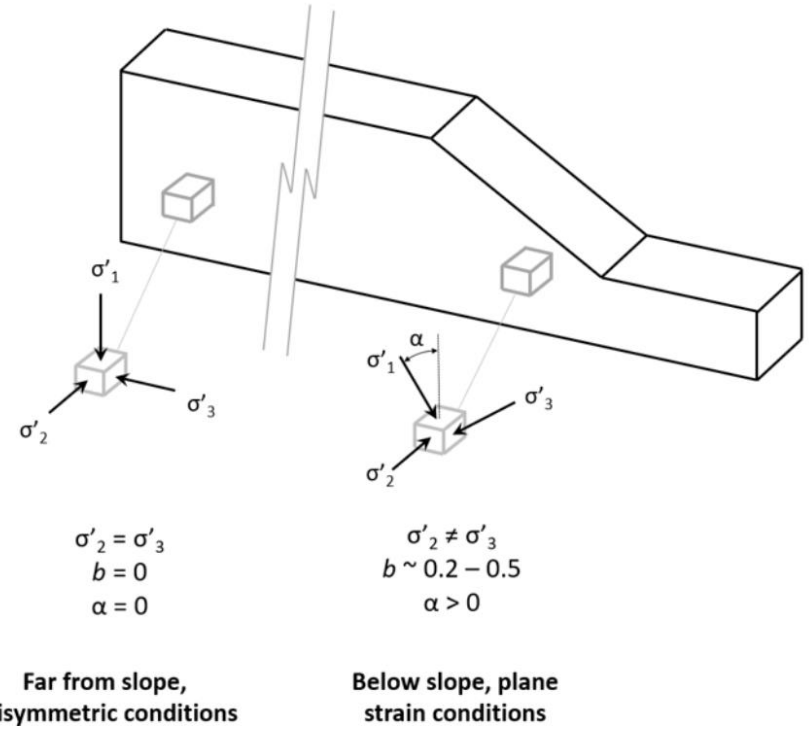

Figure 2.4. Schematic illustration contrasting axisymmetric conditions below level ground and plane strain condition below a slope (Reid et al., 2022a).

One way to account for the influence of intermediate stress is through the intermediate principal stress ratio, *b*, which can be expressed as follows:

$$b = \frac{\sigma_2 - \sigma_3}{\sigma_1 - \sigma_3} \qquad \text{Eq. 2}$$

Where, σ_1, σ_2, σ_3 are principal stress.

In axisymmetric conditions, far from slope, $b = 0$ (i.e., $\sigma_2 = \sigma_3$), whereas in the below or in proximity to slope b value ranges from 0.2 to 0.4, as observed in plane-strain testing (Wanatowski & Chu 2007, Wanatowski et al. 2010, Reid et al. 2021a).

The rotation principal stresses in the below-slope condition is not constant but gradually varies along the slope. To simulate this condition, Fanni et al (2023) prepared a TSF numerical model using the finite difference code FLAC to assess how the intermediate principal stress ratio (b) and the principal stress angles (α) develop along the critical slip surface within the tailings, as shown in Figure 2.5. The geometry adopted by the authors was chosen to provide a reasonable analogue for many upstream-raised TSFs. The tailings were modelled using the NorSand constitutive model, with parameters obtained from the Cadia Panel (Jefferies et al., 2019). As shown in Figure 5b, α ranges from zero near the surface (outside the area of influence of the slope) to about 50° near the toe. The authors also observed that the value of b along the critical slip surface is generally close to 0.3. The α values reported by Fanni et al. (2023) (0 to 50°) align with those commonly observed in the literature for below-slope stress condition (α~10-45°) (Reid, 2020).

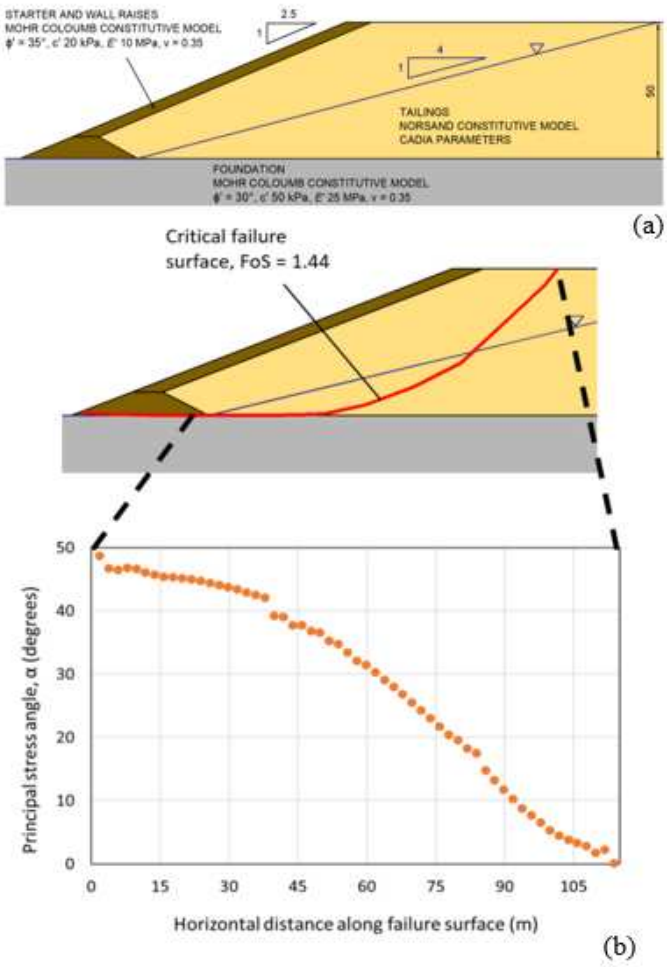

Figure 2.5. (a) TSF geometry; (b) Critical failure surface and principal stress angle along the failure surface within the tailings (after Fanni et al., 2023).

Reid (2020) compiled results from the literature on the instability stress ratio obtained under different intermediate principal stress conditions, as illustrated in Figure 2.6. In this figure, instability stress ratio was normalised to axisymmetric conditions (e.g., $b = 0$). The results indicated that instability decreased as b increased, and this effect appear to be more pronounce when α is higher. These findings further suggested that an increase in α may have increased the influence of b on instability stress ratio. (Reid, 2020).

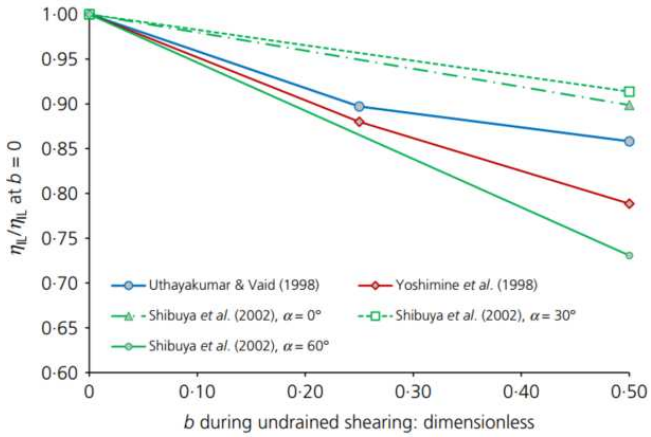

Figure 2.6. Effect of *b* on instability stress ratio (Reid, 2020).

Reid (2020) also examined the effect of principal stress direction on instability stress ratio, as illustrated in Figure 2.7. These instability stress ratios were normalized against those at an axisymmetric condition (e.g., α = 0). The results demonstrate that the principal stress angles play a significant role in the initiation of instability. The increase in α shown in Figure 2.7 promoted a significative decrease in the instability stress ratio. In practical terms, these results further indicates that static liquefaction triggering may initiate at lower values of the stress ratio. These findings show that the behaviour in the below-slope condition is quite different from those normally simulated by conventional triaxial tests and, therefore, should be taken into account in the design of tailings storage facilities.

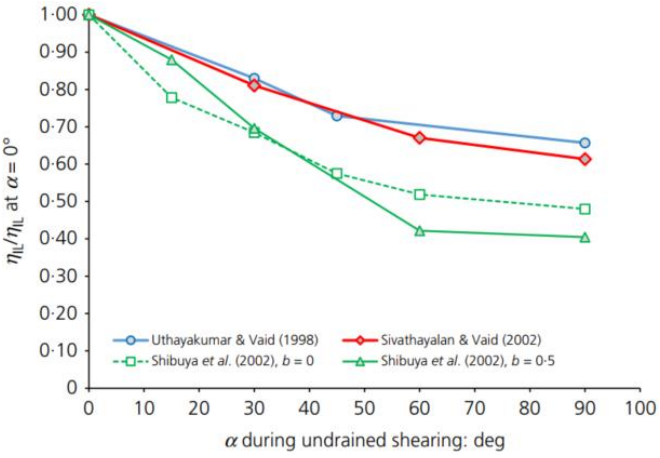

Figure 2.7. Effect of principal stress direction on instability stress ratio (Reid, 2020).

2.3. SHEAR WAVE VELOCITY FOR TAILINGS DAM MONITORING

An effective monitoring program must detect potential failure scenarios well ahead of time to enable the implementation of measures to prevent failures (Fourie et al. 2022). Forensic investigations into the Feijão dam failure, conducted by Robertson et al (2019), revealed that the installed monitoring instruments were unable to detect any notable changes prior to the failure (Ouellet et al., 2022). This analysis highlights the challenges of designing and maintaining a tailings dam monitoring system capable of providing early warning of failure (Ouellet et al., 2022).

A survey and analysis of 25 global tailings dam practitioners found that 94% consider themselves to be implementing best monitoring practices and all reported using piezometers as a primary monitoring tool, as shown in Figure 2.8 (Clarkson and Williams, 2019). Piezometers can provide indications of increasing phreatic surface such as rising water levels in the storage facility. However, using these instruments for indirect monitoring of effective stress changes within tailings storage facilities is somewhat subjective, as additional factors - such as the contrast in compressibility the tailings layers or within the foundation - add complexity to the analyses (Fourie et al., 2022). Additionally, piezometers provide point-specific measurements and may not detect a rise in the phreatic surface if not placed in the correct location.

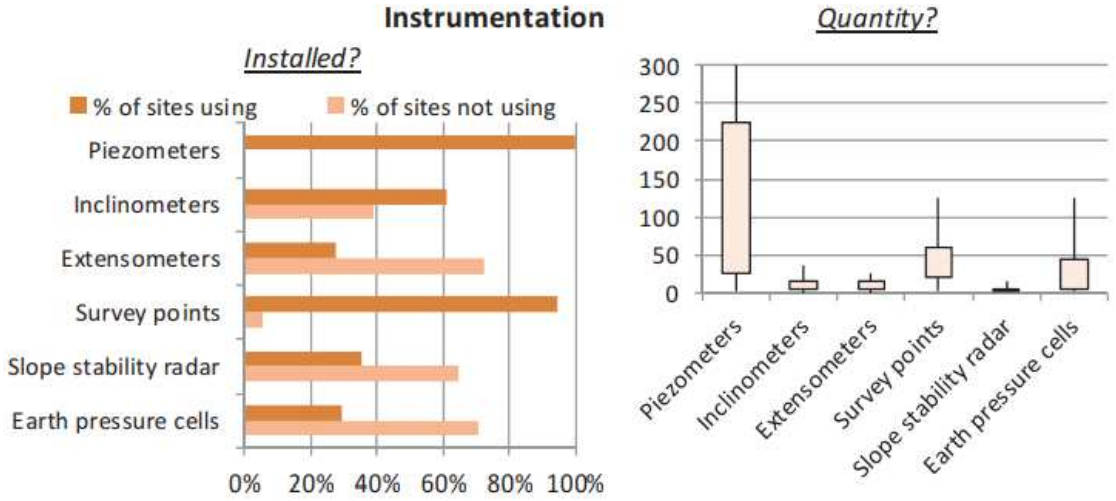

Figure 2.8. Survey results on best practice for tailings dam monitoring (Clarkson & Williams, 2019).

Jefferies et al. (2019) conducted a comprehensive investigation into the failure of the Cadia TSF. The Independent Panel noted that “piezometric data strongly suggests that

drained conditions prevailed in the tailings, and the occurrence of excess pore pressure is a consequence, not a cause, of the instability." Therefore, the deployment and monitoring of piezometers did not provide any indication of the actual stability of the embankment (Jefferies et al., 2019). This behaviour was similar to that reported by Eckersley (1990), who found that excess pore pressure arises as a consequence of static liquefaction. This does not mean that piezometers are not a valuable tool for monitoring geotechnical structures, but these studies indicate that they may not be effective in providing early warning of static liquefaction.

Monitoring of tailings dams using geophysical techniques has received increasing attention (e.g., Behm 2017; Olivier et al. 2018; Ouellet et al. 2022). One such technique, ambient noise interferometry (ANI), has been used to continuously detect temporal changes in internal seismic velocity across dams (Behm 2017; Olivier et al., 2018). This method records background vibrations and applies seismic interferometry to transform each sensor into a virtual active source (Olivier et al., 2018). However, ANI is not yet an established practice technique for tailings dam monitoring (Ouellet et al., 2022).

Recent studies have demonstrated the use of ANI in dam monitoring (e.g., Planès et al., 2016; Ouellet et al., 2022). Planès et al. (2016) used ANI to capture temporal changes in earthen embankments caused by internal erosion reporting a decrease in seismic velocity of up to 20% as internal erosion progressed. Additionally, their results showed a strong correlation between variation of V_s and pore pressure responses. Ouellet et al. (2022) demonstrated the potential of ANI for monitoring shear wave velocity (V_s) changes in TSFs, observing a strong correlation between variations in Vs and changes in the water level of the adjacent tailings pond.

Oliver et al. (2018) deployed twenty geophones along a ~ 100 m section of a gold mine TSF to record continuous seismic data. Ambient noise was used to estimate the Vs across the dam's profile. Figure 2.9 presents the V_s profile over a 20 m profile below the surface, indicating that phreatic surface approximately 10 m below the surface. A low-velocity zone near the centre of the array (between 40 and 60 m) suggests that the water table is closer to the surface in this region. These findings correlated well with cone penetration tests results performed in the area.

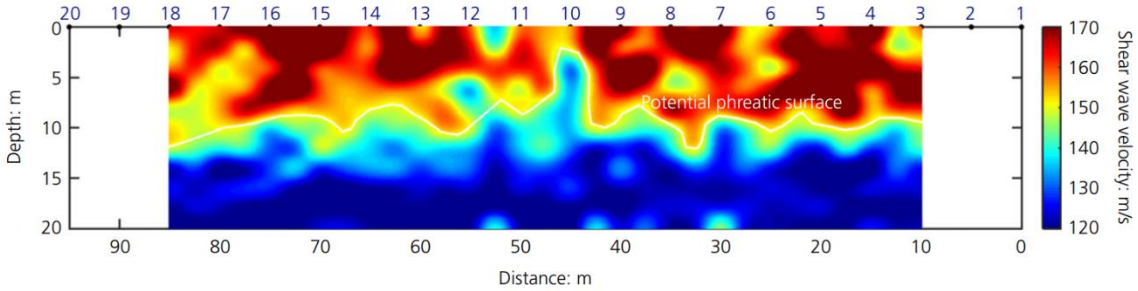

Figure 2.9. 2D shear wave velocity profile over the 95 m section (Oliver et al., 2018)

Although recent research has demonstrated the potential of using geophysical techniques to monitor stiffness variations in dams, further studies are needed to establish alert levels based on shear wave velocity changes in these structures.

CHAPTER 3

3. EXPERIMENTAL PROGRAMME

This chapter provides a brief overview of the experimental programme designed to achieve the objectives, followed by details of the methodological steps.

3.1. MATERIALS

The materials used in this study were obtained from a mine plant within Quadrilátero Ferrifero region in Minas Gerais State, Brazil. Figure 3.2 illustrates the collection, preparation and storage steps of the samples used in this study. Approximately two tons of iron ore tailings were collected from the cone pile (Figure 3.2a) and transported to the laboratory for further preparation and storage. The collected material would be deposited in a filter-stack tailings storage facility, referred to in this this study as IOT 29/87.

The SEM image obtained from IOT 29/87 reveals the shape of the particles, as shown in Figure 3.1. IOT 29/87 consists of two main types of particles: bulky dark grey particles, predominantly composed of quartz, and lighter grey particles representing haematite. The quartz particles exhibit a subangular shape, whereas haematite particles are flatter, smaller and have sharper corners. Overall, all particles exhibit high angularity, which is a characteristic commonly observed in mine tailings (e.g., Yang et al., 2019; Fourie et al., 2022).

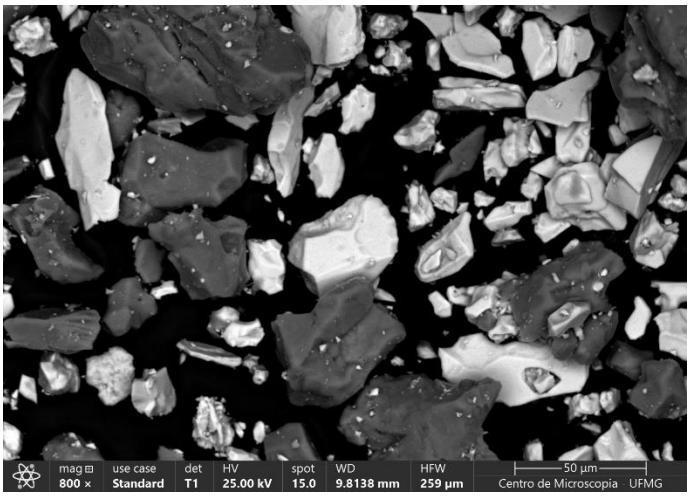

Figure 3.1. Particle morphology of IOT 29/87.

For a notation, IOT 29/87 refers the iron ore tailings with D_{50} = 29 µm and a fines content of 87 % by weight. This material was washed through an ASTM No. 200 sieve to separate the fines and then oven dried at 50 °C as illustrated in Figure 3.2b. The material retained on sieve No. 200 was labelled IOT 94/12, whereas the material passing through the sieve was labelled as IOT 29/98. Figure 3.2c illustrates the process of storing samples in plastic bags. Figure 3.2d shows the materials storage in metal drums for transportation to Australia by air.

Figure 3.2. Sample preparation: (a) Collection at the processing plant; (b) Washing to separate fines; (c) Drying and storage in plastic bags; (d) Storage in metal drums for later transportation.

IOT 89/30 IOT and IOT 62/55 were obtained by blending IOT 94/12 and IOT 29/98. Figure 3.3 illustrates that IOT 29/98 has a darker colour than IOT 94/12 due to mineralogical differences between them. The darker material is rich in iron ore oxides, whereas the lighter material has a higher quartz content. These mineralogical differences will be discussed in more detail later.

Figure 3.3. Sample mixing process.

The particle size distribution and the index properties of the iron ore tailings studied are presented in Figure 13 and Table 1, respectively. Particle size distribution was determined in accordance with Australian Standard AS 1289.3.6.1 (2009) and AS 1289.3.6.3 (2003), whereas specific gravity was measured following AS 1289.3.5.1 (2006). The chemical composition was determined using XRF (X-ray fluorescence) analysis, revealing the predominant presence of haematite (Fe_2O_3) and quartz (SiO_2).

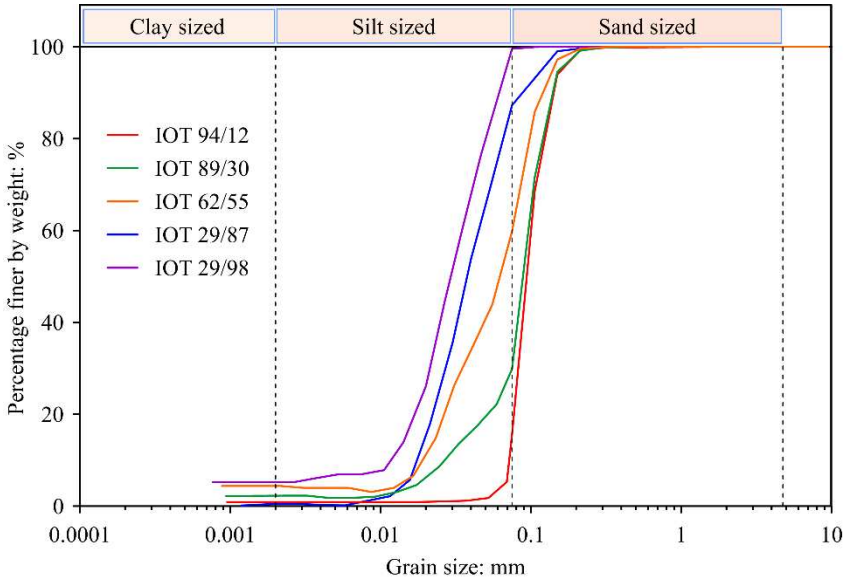

Figure 3.4. Particle size distribution of the iron ore tailings studied.

Table 3.1 shows that the uniformity coefficient also varies with fines content, increasing up to 55% before decreasing and then remaining constant at higher fines content. All materials

were classified as non-plastic. Additionally, a gradual increase in specific gravity is observed as fines content increases. This trend appears to be associated with changes in mineral composition. This interpretation is supported by the findings of Espósito (2000), who examined iron ore tailings from the Quadrilátero Ferrífero and demonstrated a linear relationship between iron content and specific gravity, as shown in Figure 3.5. It is observed that the results from the present study are consistent with those reported by Espósito (2000).

Table 3.1. Index properties of iron ore tailings studied

Iron ore tailings mixtures		94/12	89/30	62/55	29/87[(1)]	29/98
Median grain size D_{50}: mm		0.094	0.089	0.062	0.029	0.029
Percentage passing 200 sieve		12	30	55	87	98
Specific gravity, Gs		2.76	2.87	3.08	3.36	3.50
Uniformity coefficient D_{60}/D_{10}		1.4	3.5	3.9	2.9	2.9
Chemical composition	Fe_2O_3 (%)	8.0	19.6	27.6	40.2	47.5
	SiO_2 (%)	91.8	80.1	72.0	58.2	51.0
	Other elements (%)	0.2	0.3	0.4	0.6	0.5

[(1)] 29/87 represents a median grain size D_{50} of 29 μm and a fines content of 87%.

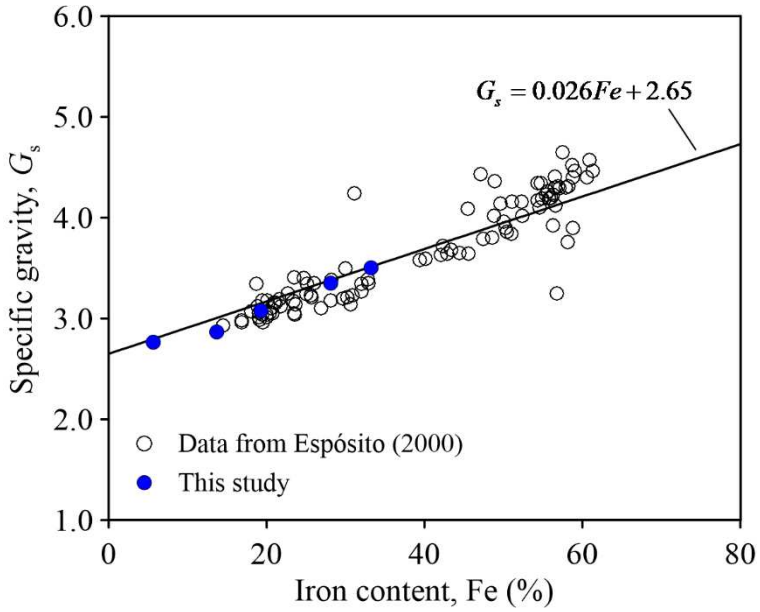

Figure 3.5. Relationship between specific gravity and iron content

3.2. TESTING PROCEDURES

To achieve the objectives of this research, high-quality testing protocols were adopted for all laboratory experiments. Table 3.2 summarises the full programme of triaxial compression, hollow cylinder and bender elements tests carried out on the studied iron ore tailings. All these tests were performed at the Soil Mechanics Laboratory of The University of Western Australia

(UWA). One of the primary objectives of this study was to examine behaviour over a range of void ratios, confining stress, specimen preparation techniques, and fines contents. Furthermore, the role of stress rotation and intermediate principal stress in instability stress ratio was investigated.

Table 3.2. Laboratory test programme for the iron ore tailings studied

Iron ore tailings mixtures	94/12	89/30	62/55	29/87	29/98
CIU tests	6	2	4	4	2
CAU tests				16	
CID tests	14	8	11	14	14
HCTS tests				17	
Bender/CSD tests				5	
Resonant column tests	1	1	1	1	1

3.2.1. TRIAXIAL COMPRESSION TEST

The aim of triaxial tests was to evaluate the behaviour of the studied tailings from a wide range of state parameters. The loose specimens contributed to obtaining the critical state line in the *e-p*' plane, whereas dense specimens were used to obtain the CSL in *q-p*' plane. All tests followed the protocols recommended in Appendix B of Jefferies and Been (2015).

Figure 3.6a-d illustrates the step-by-step procedure for preparing and executing the triaxial compression tests. At the top of Figure 3.6a are the tamper and the split mould used during the moist tamping preparation, whereas below are the grease tube, discs of standard triaxial latex membrane, porous stones, filter papers, and the base and top platens. Both platens are oversized and lubricated to reduce strain non-uniformity and the influence of platen restraint on stress in the specimens (Rowe and Barden 1964). An oversized platen means that the diameter of the platens is slightly larger than the specimen diameter. This ensures full support during shearing and allows uniform radial deformation throughout the specimen (Viana da Fonseca et al., 2021). To facilitate the freezing process at the end of the test, Reid et al. (2021b) designed a stiff, smooth, oversized platen, that allows a specimen to be placed in the freezer without transferring the entire triaxial base.

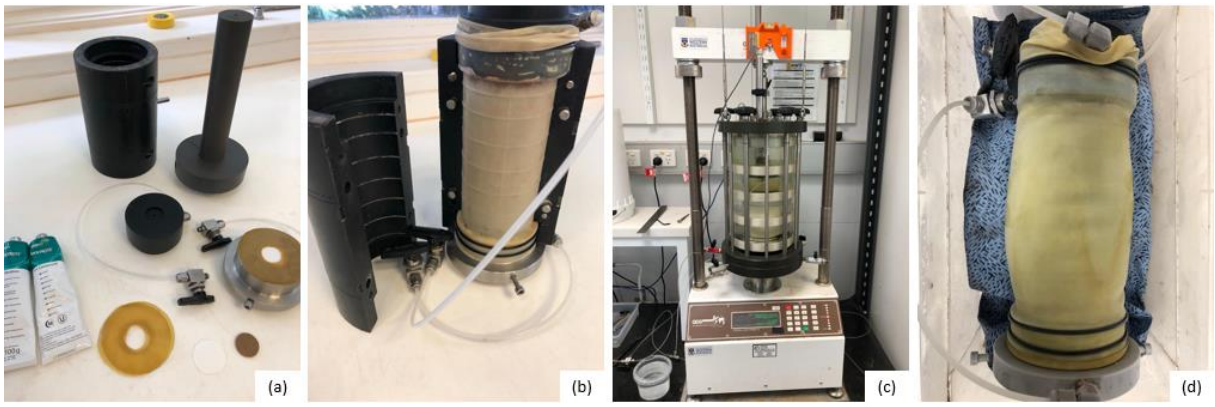

Figure 3.6. (a) Items used for specimen preparation; (b) Split mould and specimen prepared for testing; (c) Triaxial compression test setup; (d) Specimen after freezing at the end of the test.

The preparation of top and bottom platens consisted, initially, of cleaning the surface and coating it with a thin vacuum grease. Next, the first latex disc was placed on the lubricated surface, and the second thin coat of vacuum grease was placed over it. The last step was placing the second latex disc over the first. After this was completed, a thin coat of silicone grease was applied around the platen to seal it and prevent leaks during the tests. The bottom part of the membrane specimen was stretched and placed around the bottom platen, and some O-rings were also used to prevent leaks.

Figure 3.6b illustrates the split mould and specimen prepared for triaxial testing. This mould has a grid of small channels designed to distribute the vacuum throughout its internal face. The vacuum between the internal face of the mould and the membrane was applied to stretch the triaxial membrane, holding it against the mould during the tamping process. A suction cap and the conical extension were used to connect the top platen to the internal submersible load cell, preventing tilting of the top platen during shearing, as recommended by Reid et al. (2021c). Misalignment of the specimens during the test results in a non-perpendicular loading, which produces non-uniform strains and stress during the shearing (Viana da Fonseca et al., 2021).

The moist tamping (MT) technique was employed to obtain loose specimens. Initially, each material was moistened to a gravimetric moisture content of about 3% and thoroughly mixed before being left in a covered container for at least 24 hours to allow moisture content equalisation before testing. This curing process is essential to ensure that the fines particles in the sample become properly wetted (Jefferies and Been, 2015). The specimens were lightly tamped in eight layers of equal volume, using an undercompaction ratio of 3% to improve

specimen uniformity, following the procedure recommended by Ladd (1978). The top of each layer was carefully scarified before placing the next layer to promote better bonding between the layers. At the end of specimen preparation, a small vacuum (negative pore pressure equal to 15 kPa) was applied to the specimen to keep its shape and remove mould. Each test was carried out on specimens of 70 mm diameter and 140 mm high, approximately.

The triaxial compression tests were performed in a standard triaxial device manufactured by GDS Instruments Ltd (GDS), as illustrated in Figure 3.6c. This device allows control of the cell and back pressure/volume, load frame and the testing rate.

Complete saturation of the specimens is essential for adequately assessing the CSL, and using carbon dioxide (CO_2) before water flushing aids in this process (Viana da Fonseca et al., 2021). A low-pressure CO_2 source (< 3 kPa) was intruded into the bottom drainage line, and the bubble rate rising through the tube from the top platen drainage line was monitored. A bubble ratio of less than one to five bubbles per second was used to control the CO_2 pressure, as recommended by Jefferies and Been (2015). After use of CO_2, the specimens were flushed with deaired deionised water, and subjected to back-pressure saturation to provide a full saturation condition. The specimen saturation step was finalized when the Skempton's coefficient B reached 0.98 or higher.

Measurement of the void ratio of sand specimens in the triaxial test can be subject to significant errors (Jefferies and Been, 2016). Sladen and Handford (1987) proposed the end-of-test soil freezing technique to measure the final water content. Applying this method leads to reliable measurements of the void ratio after testing, which allows to obtain also more reliable CSL (Viana da Fonseca et al., 2021). In the present study, a modular base platen system designed by Reid et al. (2021b) was used for freezing the specimens. After testing, this device allows the entire specimen to be manually removed and placed in the freezer, as illustrated in Figure 3.6d. After this process it is possible to obtain the specimen end-of-test void, knowing the water content measured and the material's specific gravity, G_s, By knowing the void ratio post-test measurement and the volume changes of the specimen during shearing, it is also possible to obtain the void ratio at the end of consolidation.

While moist tamping (MT) was used to prepare loose specimens, the "air-dried" (AD) technique was employed to produce dense specimens. This method produces more uniform specimens without exposing them to tamping-induced stress (Reid et al., 2024). Tamping-induced stresses can result in changes to the stress–strain and peak undrained strength,

producing nonconservative strength results (Reid et al., 2022b). Reid et al. (2022c) described a procedure where slurry is poured into a bucket and left to dry until the water content becomes suitable for specimen trimming. Each iron ore tailings sample outlined in this study was mixed with amount of water to achieve a water content of around 28%, producing the thinnest possible slurry without segregation after pouring, as illustrated in Figure 3.7a. Different water contents were tested before defining it. It is important to highlight that the reduction in the fines content has reduced the water content required to produce thick slurry. Figure 3.7b shows the 10L bucket with geotextile affixed to its inner surface, which provides a drainage path length and helps ensure near-uniformity of water content throughout the block, as recommended by Reid et al. (2022c; 2024). The slurry was then poured into the bucket (Figure 3.7c), and the densification process was carried out by gently tamping around the bucket with hands. This bucket was placed in an oven at 50ºC (Figure 3.7d) until the specimen reached a water content of around 12%, allowing it to form a freestanding block when inverted onto a table. Cylindrical specimens were carefully trimmed using a stainless-steel tube with sharp cutting edge.

Figure 3.7. Preparation steps of the dense specimens using the “Air dried” technique.

3.2.2. HOLLOW CYLINDER TEST

The stress-strain-strength behaviour of soils in below-slope condition cannot be investigated in a triaxial testing apparatus, as it cannot apply principal stress rotation or shear at principal stress angles relevant to stress conditions (Fanni et al., 2023). The torsional shear hollow cylinder (TSHC) apparatus can simulate below-slope conditions; however, studies on tailings remain limited (Fanni et al., 2023).

Hollow cylinder tests were performed in a device manufactured by GDS Instruments. The tests were carried out in specimens with an outer diameter of 100 mm, an inner diameter of 60 mm, and a hight of 200 mm, approximately. Pressure pumps control and measure the cell, inner and back pressures, while a submersible multiaxial load cell controls and records the axial and torque loads. The brass porous stones used in this device feature small stainless-steel ribs to improve contact with the specimen (Fanni et al., 2024). Figure 3.8 and Table 3.3 present the stress conditions and the equations used to assess stress and strain in the hollow cylinder test, respectively.

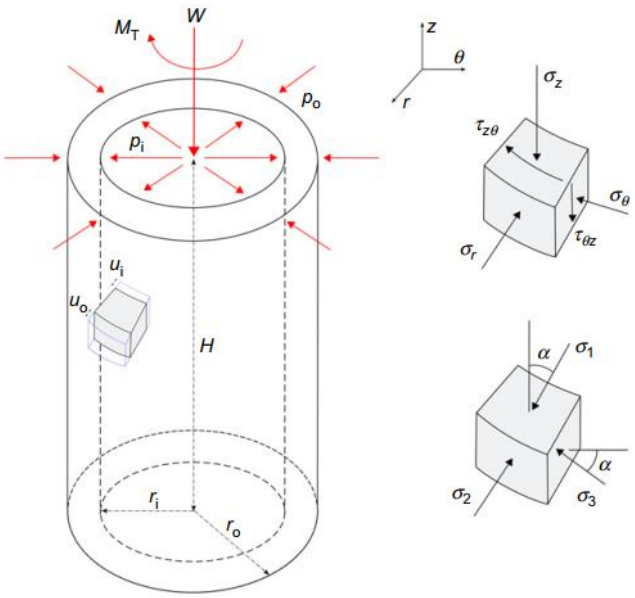

Figure 3.8. Stress conditions in hollow cylinder tests (Fanni et al., 2024a).

Table 3.3. Hollow cylinder tests: stresses and strains formulations (Fanni et al., 2024)

Parameter definition	Stresses	Strains
Vertical	$\sigma_z = \frac{W}{\pi(r_o^2 - r_i^2)} + \frac{p_o r_o^2 - p_i r_i^2}{r_o^2 - r_i^2}$	$\varepsilon_z = -\frac{\Delta H}{H}$
Radial	$\sigma_r = \frac{p_o r_o + p_i r_i}{r_o + r_i}$	$\varepsilon_r = -\frac{u_o - u_i}{r_o - r_i}$
Circumferential	$\sigma_\theta = \frac{p_o r_o - p_i r_i}{r_o - r_i}$	$\varepsilon_\theta = -\frac{u_o + u_i}{r_o + r_i}$
Shear	$\tau_{z\theta} = \frac{3M_T}{2\pi(r_o^3 - r_i^3)}$	$\gamma_{\theta z} = \frac{2\theta(r_o^3 - r_i^3)}{3H(r_o^2 - r_i^2)}$
Major principal	$\sigma_1 = \frac{\sigma_z + \sigma_\theta}{2} + \sqrt{\left(\frac{\sigma_z - \sigma_\theta}{2}\right)^2 + (\tau_{z\theta})^2}$	$\varepsilon_1 = \frac{\varepsilon_z + \varepsilon_\theta}{2} + \sqrt{\left(\frac{\varepsilon_z - \varepsilon_\theta}{2}\right)^2 + \left(\frac{\gamma_{\theta z}}{2}\right)^2}$
Intermediate principal	$\sigma_2 = \sigma_r$	$\varepsilon_2 = \varepsilon_r$
Minor principal	$\sigma_3 = \frac{\sigma_z + \sigma_\theta}{2} - \sqrt{\left(\frac{\sigma_z - \sigma_\theta}{2}\right)^2 + (\tau_{z\theta})^2}$	$\varepsilon_3 = \frac{\varepsilon_z + \varepsilon_\theta}{2} - \sqrt{\left(\frac{\varepsilon_z - \varepsilon_\theta}{2}\right)^2 + \left(\frac{\gamma_{\theta z}}{2}\right)^2}$
Deviatoric stress triaxial	$q_{13} = \sigma_1 - \sigma_3$	
Deviatoric stress octahedral/Octahedral shear strain	$q = \frac{1}{\sqrt{2}}\sqrt{(\sigma_1 - \sigma_2)^2 + (\sigma_2 - \sigma_3)^2 + (\sigma_3 - \sigma_1)^2}$	$\gamma_{oct} = \frac{2}{3}\sqrt{(\varepsilon_1 - \varepsilon_2)^2 + (\varepsilon_2 - \varepsilon_3)^2 + (\varepsilon_3 - \varepsilon_1)^2}$
Mean effective stress	$p' = \frac{\sigma_1' + \sigma_2' + \sigma_3'}{3} = \frac{\sigma_z' + \sigma_r' + \sigma_\theta'}{3}$	
Intermediate principal stress ratio	$b = \frac{\sigma_2' - \sigma_3'}{\sigma_1' - \sigma_3'}$	
Principal stress angle	$\alpha = \frac{1}{2}\arctan\left(\frac{2\tau_{z\theta}}{\sigma_z - \sigma_\theta}\right)$	
Stress ratio Volumetric strain	$\eta = \frac{q}{p'}$	$\varepsilon_{vol} = -\frac{\Delta V}{V}$

Table 3.3 shows that the deviatoric stress formulation used in hollow cylinder tests (q) differs from that commonly used in triaxial testing (q_{13}). In the hollow cylinder tests, q is referred to as octahedral deviatoric stress and accounts the effect of the intermediate principal stress. The stress ratio at instability in hollow cylinder tests was calculated using octahedral deviatoric stress, as recommended by Fanni et al. (2024a).

The MT technique was used to prepare loose specimens, while AD was used to achieve denser states. HCTS tests were performed on samples of IOT29/87. Figure 3.9 illustrates the steps to prepare MT specimens. These specimens were prepared in ten layers at a gravimetric water content of 3%. An undercompaction ratio of 3% to improve specimen uniformity (Ladd, 1978). The top of each layer was carefully scarified before placing the next layer to promote better bonding between the layers. A suction of approximately 30 kPa was applied inside the specimen to allow removal from the split mould and to measure of the initial specimen dimensions using a pi tape.

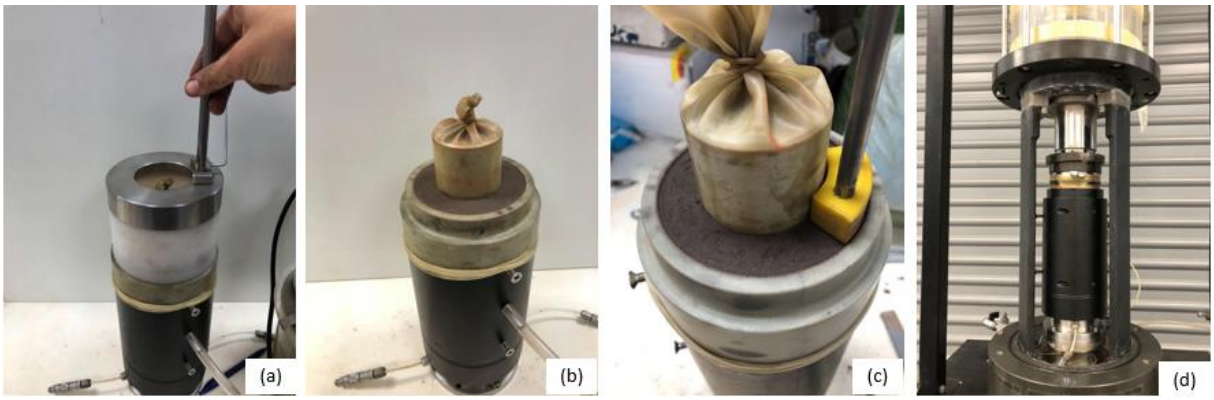

Figure 3.9. Preparation steps of test specimens using the MT technique for hollow cylinder tests.

Specimen preparation using the AD technique for hollow cylinder tests follows almost the same as for triaxial tests, except for the trimming process, as illustrated in Figure 3.10. As shown in Figure 3.10b, specimens were carefully excavated to form an inner cavity using a small hand-held auger designed by GDS Instruments (GDS). Then, they were set up in the hollow cylinder apparatus.

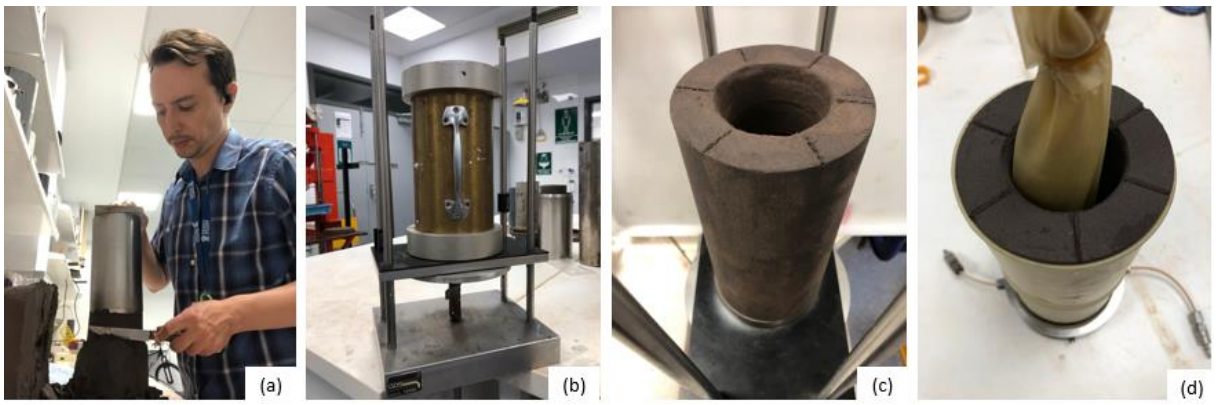

Figure 3.10. Preparation steps of test specimens using the AD technique for hollow cylinder tests: (a) specimen trimming; (b) excavation of the interior specimen; (c) trimmed and excavated specimen; (d) Specimen with external and internal membrane installed.

All specimens were firstly flushed with CO_2, then deionized and deaired water was supplied until air bubbles no longer rose from the specimen. The back-pressure was gradually increased until a Skempton's B-value of ≥ 0.98 was achieved. Specimens were consolidated anisotropically under a relationship between horizontal and vertical stress, K_c, of 0.70. This adopted K_c value has been commonly used in previous tailings studies (e.g., Jefferies and Been, 2115; Reid et al., 2022). Consolidation was carried out by progressively ramping p' at a rate of 8 kPa/hour, as recommended by Fanni et al. (2023). During drained or undrained shearing, a

strain rate equal to 0.34%/min was applied, consistent with previous hollow cylinder tests on silty tailings (e.g., Fanni et al., 2023).

During this experimental program, both drained and undrained tests were performed. The drained tests aimed to evaluate the uniqueness of CSL in the e-*p*' plane with respect to variation of α and b, whereas the undrained tests were carried out to investigate the influence of α and *b* on the undrained behaviour of tailings. Values of α = 22.5º, and 45º and *b* = 0.3 and 0.5 were used in this study. These range of α and *b* have been used to represent the below-slope stress conditions (Reid, 2020; Fanni et al., 2025).

Fanni et al. (2023) reported unsuccessful attempts to adopt freezing specimen at end of testing to measure the gravimetric water content, as the specimen bonded to the sintered brass porous stone and inner membrane upon frozen. Instead, void ratio at end of testing was measured using the procedure described by Fanni et al. (2023). These authors proposed a simple method for determining the void ratio at end of testing in hollow cylinder tests. This method requires measuring the masses of the entire setup, including the outer and inner membranes, platens, porous stones, screws, O-rings, grease, and the water within drainage lines.

After testing, the shutoff valves on the drainage line are released (without losing of water and soil particles) and any water present outside the membranes need to be carefully removed, allowing to measure the total mass (shown in Figure 3.11c). The mass of the saturated specimen is determined by subtracting the mass of the setup from the total measured mass after the testing. The dry mass is measured by a carefully washing the tailings (without losing particles) within the membranes into a tray and then placed in an oven at 105ºC for 24 hours (shown in Figure 3.11d).

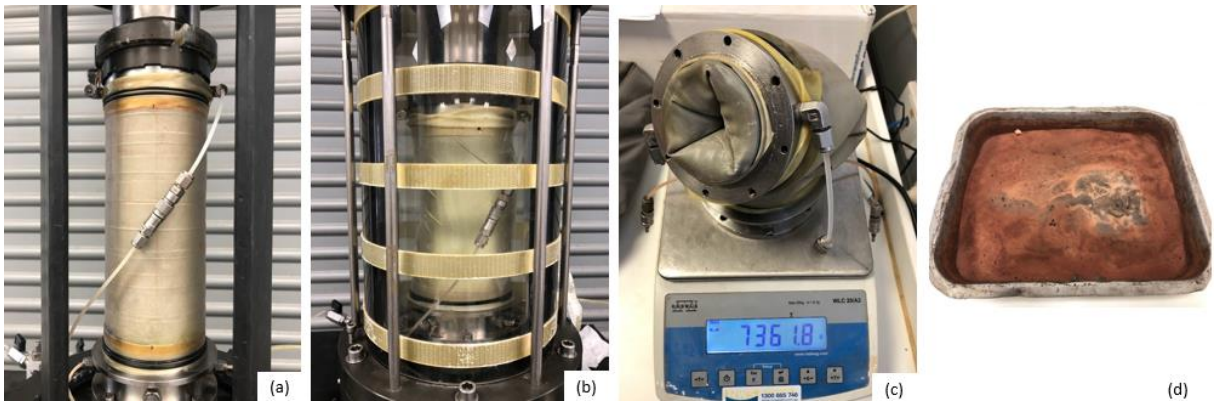

Figure 3.11. Steps of the HCTS test: (a) Specimen installation in the device; (b) Test execution; (c) Total mass after the test; (d) Specimen dried in an oven for 24 hours.

3.2.3. BENDER ELEMENTS IN CSD STRESS PATH

A series of bender elements tests were carried out during triaxial shearing under a CSD stress path to demonstrate the potential of geophysical techniques to monitor stiffness variations in tailings. These tests were performed using a GDS triaxial device, as illustrated in Figure 3.13, on specimens of 50 mm diameter and 100 mm high, approximately. Loose specimens were moist tamping, whereas dense specimens were prepared using the dried method, following the previously described procedures. Saturation procedures involved CO_2 flushing, water percolation and back-pressure saturation was applied until a Skempton's B parameter > 0.98 was achieved.

Figure 3.12 illustrates the stress paths adopted in this study, shown in q-p' plane. Specimens were anisotropically consolidated under consolidation stress ratio ($K_c = \sigma_3/\sigma_1$) of 0.7. Drained shearing along Stress path C was carried out under strain-controlled shearing at a rate of 0.02 mm/min for 120 min. During the test, the mean effective stress (p') was reduced at a rate of 0.5 kPa/min under drained conditions (with open drainage valves), and no excess pore pressure was observed. An advanced GDS apparatus was used, allowing real-time updates of the cross-section area during shearing. This correction is fundamental to ensuring a constant q throughout the test (Rabbi et al. 2019). Shear wave velocity measurement was obtained during the drained shearing, creep, and CSD stages.

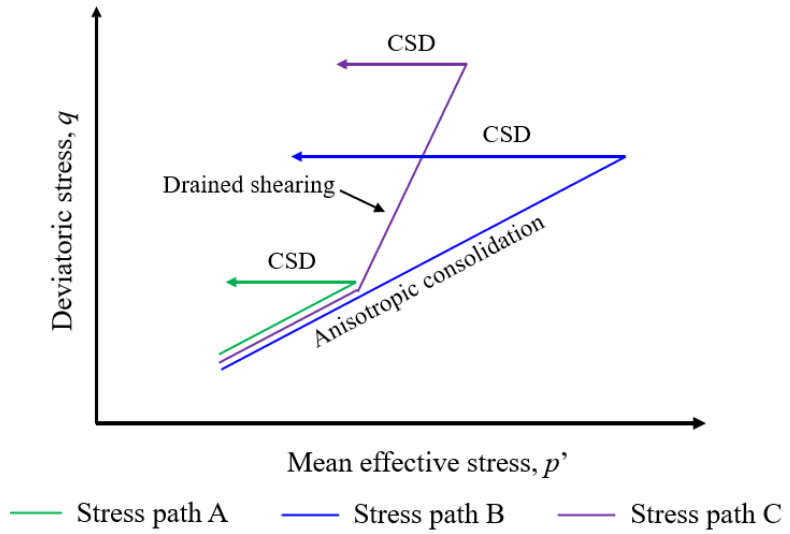

Figure 3.12. Schematic of CSD stress-paths used in this study

The shear wave travel time (t) was estimated as the time between the start of the voltage pulse and the first deflection in received output signal from the bender elements. Eq. 1 was used to estimate shear wave velocity and small-shear modulus. During shear wave propagation, the applied pulse also generates a compression wave component, known as the near-field effect. This phenomenon might lead to misinterpretation of travel time (Leong et al., 2009). To minimise the distortions associated with this effect in Vs measurements, a wide range of sinusoidal pulses at various frequencies (i.e, 1 to 20 kHz) were applied, and the procedure recommended by Leong et al (2005) and Viana da Fonseca et al. (2009) was adopted

$$G_0 = \rho V_s^2 \text{ with } V_s = L_{tt} / t \qquad 1$$

where ρ is the soil density; L_{tt} is the wave path length, which is taken as the distance between the tips of the source and receiver bender elements; and t is the shear wave travel time.

Figure 3.13. CSD test with shear wave velocity measurements.

End-of-test soil freezing is incompatible with the bender elements due to the potential for damaging the piezoelectric transducers during the freezing process (Viana da Fonseca et al. (2021). Instead, the void ratio at the end of testing was determined using the procedure recommended by Verdugo and Ishihara (1996). After testing, cell pressure is increased under drained conditions (with open drainage valves). The valves are closed, and the cell pressure is rapidly reduced to generate a suction within the specimen, facilitating its recovery for oven-drying (Verdugo and Ishihara, 1996).

3.2.4. RESONANT COLUMN TESTING

A series of resonant column (RC) tests were carried out in this study to evaluate the shear wave velocity of all mixtures. A Stoke-type apparatus manufactured by GDS instruments was used, as illustrated in Figure 3.14. Specimens were prepared in a loose state using the moist tamping technique. After test setup, the rigid cylindrical chamber was closed and the specimen isotropically consolidated until the target *p*' prior to testing. During the test, a torsional excitation with a very low voltage (0.002 V) was applied to ensure that the induced shear strain remained below the elastic threshold (typically around 0.001% for sands) (Cho et al., 2006).

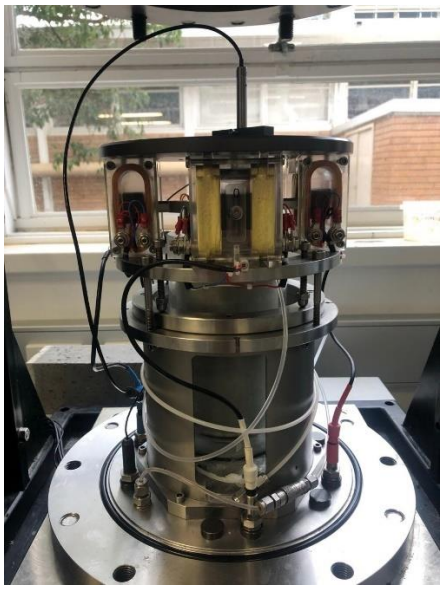

Figure 3.14. Resonant column apparatus

To obtain a more accurate measurement of void ratio at the end of the test, an apparatus developed by Vulpe (2024) was used. This device allows the specimen to be moved to a freezer, following a procedure similar to that described previously for triaxial compression testing.

CHAPTER 4

4. RESULTS AND DISCUSSION

This chapter presents the results and discussion of the triaxial compression, hollow cylinder, and bender element tests conducted in this study.

4.1. INFLUENCE OF GRADING ON CRITICAL STATE BEHAVIOUR

The critical state line depends on intrinsic particle characteristics such as particle shape, grading, and mineralogy (Fourie et al., 2022). To illustrate the effect of gradation, triaxial compression tests were carried out on the studied tailings. The projections of the critical state line in the *e*-*p*' and *q*-*p*' planes are presented in Figure 4.1 and Figure 4.2, respectively. These projections were defined using the critical friction ratio (M_{tc}) and a power-law model as proposed by Li and Wang (1998), which can be expressed as follows:

$$e_{cs} = e_r - \lambda_c \left(\frac{p'}{p_{ref}} \right)^{\xi} \qquad 2$$

Where: e_r, λ_c, and ζ are fitted parameters; and p_{ref} is the reference stress equal to 100 kPa.

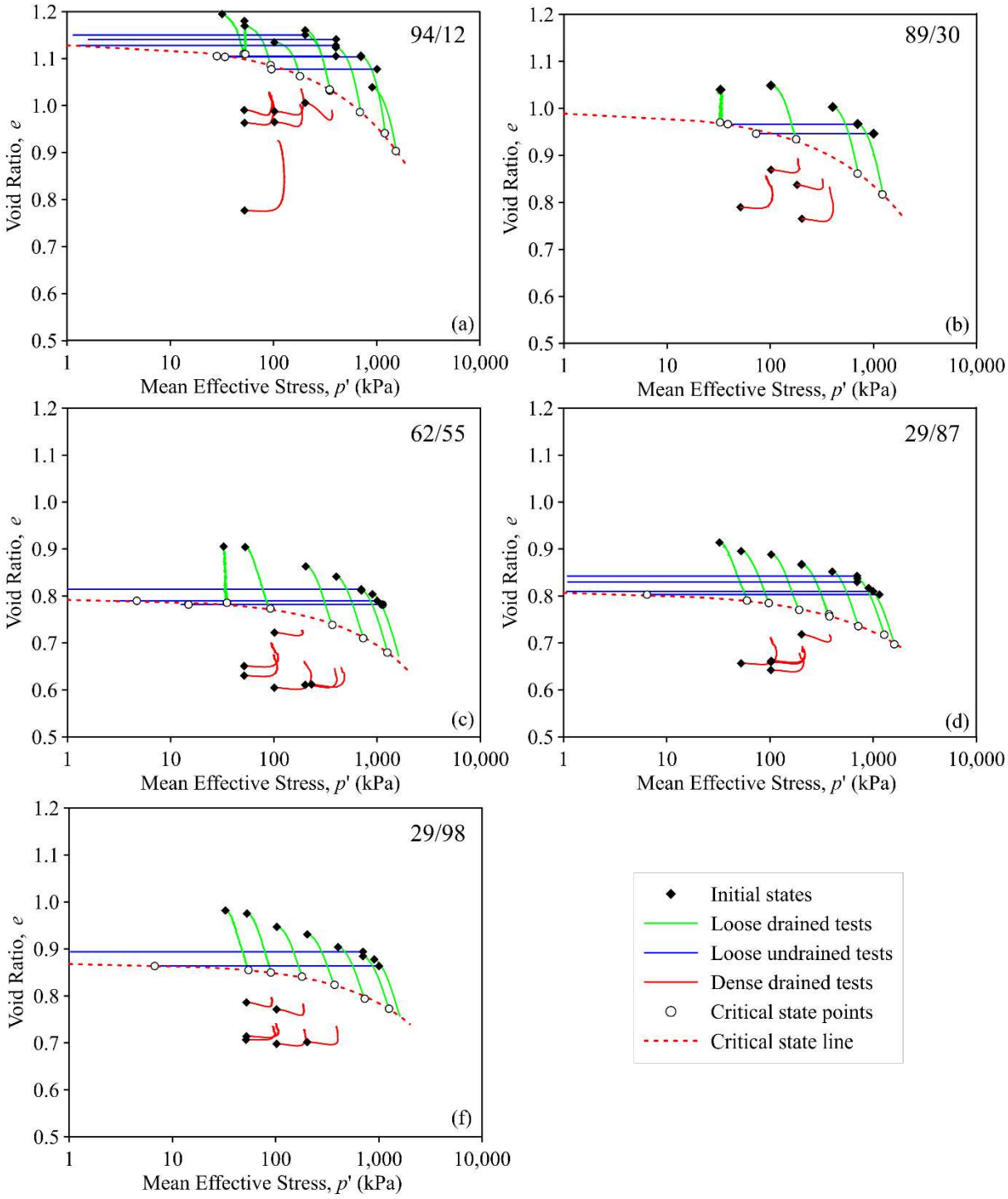

Figure 4.1. Effect of grading in critical state line in e-p' plane.

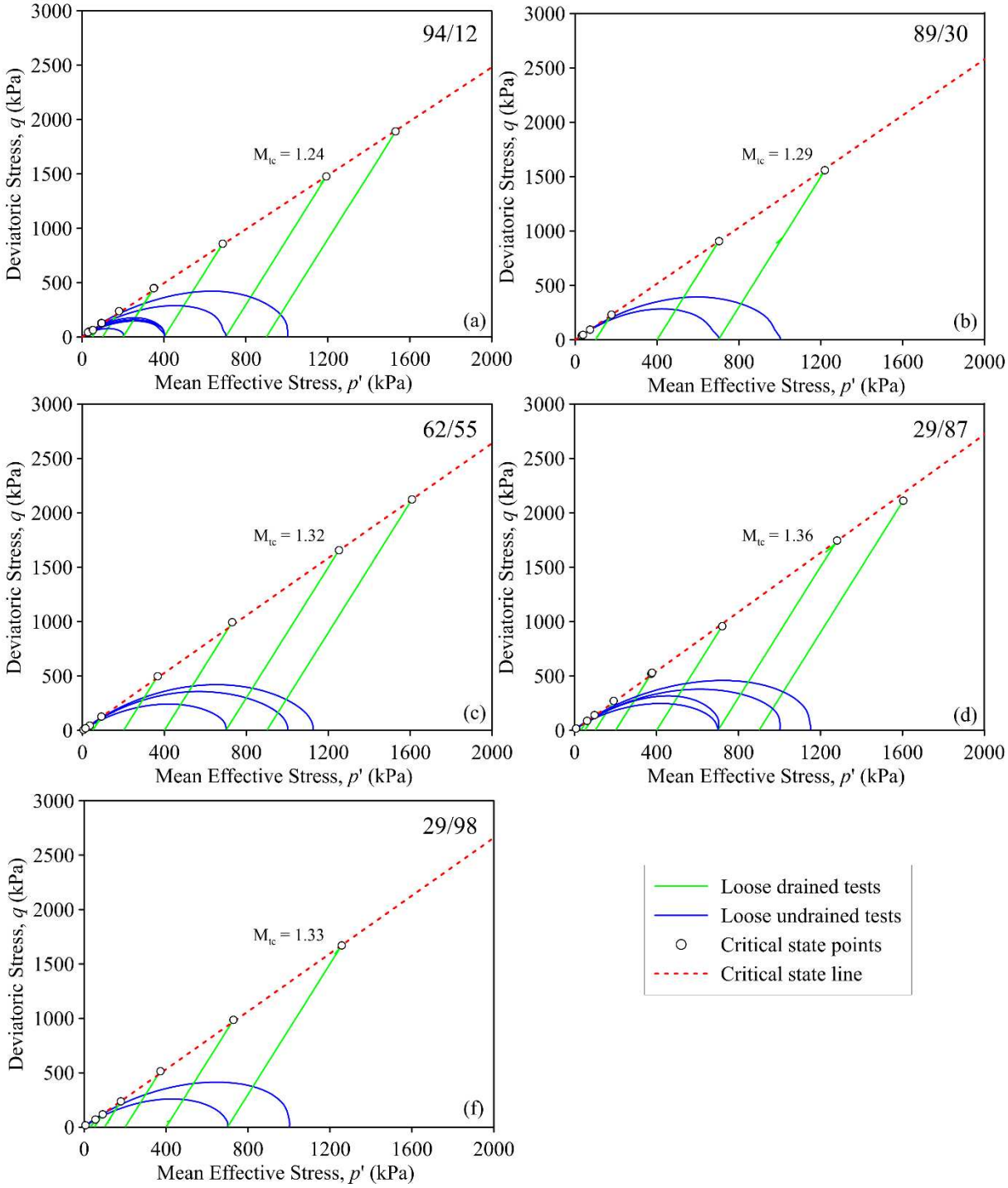

Figure 4.2. Effect of grading in critical state line in q-p' plane.

The critical state fitting parameters are summarized in Table 4.1. The results show that the loose specimens reached the CSL, whereas the dense specimens (indicated by red lines) progressed towards it but did not achieve the critical state. In drained conditions, dense specimens may develop shear zones in which the local void ratio is higher the global average measured using the entire specimen at the end of testing (Jefferies and Been, 2015).

Table 4.1. Critical state lines in e-p' and q-p' planes

Iron ore tailings mixtures	$e-p$' plane			$q-p$' plane
	e_r	λ	ζ	M_{tc}
94/12	1.132	0.048	0.569	1.24
89/30	0.993	0.046	0.535	1.29
62/55	0.793	0.023	0.630	1.32
29/87	0.809	0.026	0.518	1.36
29/98	0.869	0.021	0.606	1.33

The CSLs of the different mixtures are presented in Figure 4.3a and Figure 4.3b. Figure 4.3a shows that, in the *e–p′* plane, the CSL shifts downward as fines content increases but moves upwards when the fines content exceeds 55%. This pattern is consistent with findings from previous studies on tailings (e.g. Carrera et al., 2011; Torres-Cruz and Santamarina, 2020). For example, Carrera et al. (2011) carried out monotonic triaxial tests on sand-silt mixtures obtained from the Stava tailings storage facility and found that increasing silt content caused the CSL in the *e-p*' plane to shift downwards until an inversion occurred at a fines content of 50%. According to Thevanayagam et al. (2002), this inversion is related to changes in particle interactions. At low fines content, contacts occur predominantly between coarse particles, whereas at high fines content, interactions are primarily between fine particles. As the fines content increases, the finer particles fill the voids and progressively separate the coarse particles, reducing contact between them. In this case, fine particles begin to actively participate in the internal force chain within the mixture. Therefore, the results presented in Figure 4.3a suggest that for fines contents lower than 55% the behaviour is mainly dominated by the contact between the coarse particles, whereas at higher fines contents, the finer particles begin to control the behaviour of the mixtures, leading to the inversion of the CSL in the *e-p*' plane.

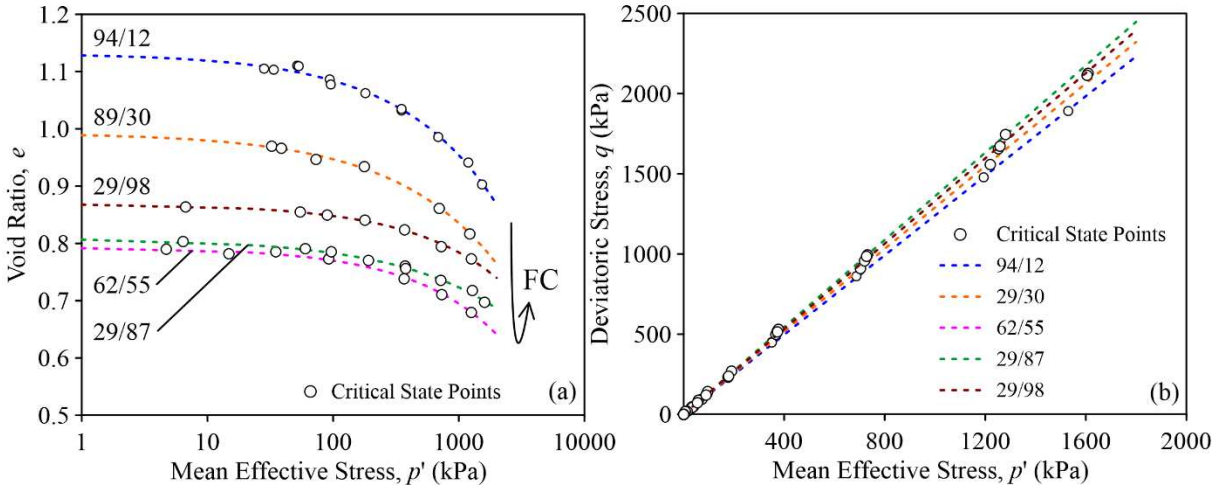

Figure 4.3. Critical state points from all tests presented in: (a) the e–p′ plane; and (b) the q–p′ plane.

As observed in Figure 4.3b the CSL in the *q*-*p*' plane is influenced by gradation effects. The critical friction ratio (M_{tc}) tends to increase as the fines content increases up to FC = 87%, decreasing slightly for even higher fines contents. Carrera et al. (2011) and Torres-Cruz and Santamarina (2020) reported that M_{tc} varies slightly with the addition of fines.

Figure 4.4 illustrates the influence of increasing fines content on critical friction ratio (M_{tc}), mineralogy and grain shape. The particle images were obtained using back-scattered electron (BSE) under scanning electron microscopy (SEM). The increase of fines promotes an increase in hematite (lighter grey particles). These finer, platy particles exhibit sharp edges, very low sphericity and roundness, and high angularity and with rough surfaces. Inter-particle friction generally increases with surface roughness (Jeng et al., 2019) and decrease with roundness (Cho et al., 2006). Therefore, the observed increase in M_{tc} is associated with the greater amount of hematite particles. The slight reduction in M_{tc} for the 29/98 mixture suggests that the coarse quartz particles also contribute to inter-particle friction.

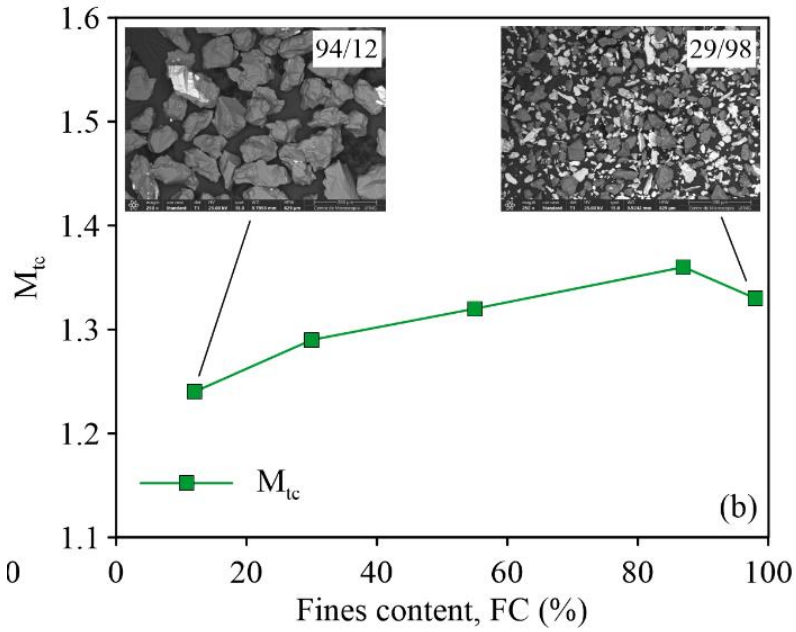

Figure 4.4. Effect of fines content on critical friction ratio (M_{tc})

The critical friction ratio dependents on both mineral-mineral friction and also the particle shape (Cho et al., 2006). In general, the mineralogy and particle shape of tailings within a storage facility are sufficiently constrained to prevent significant variations in M_{tc} (Fourie et al., 2022). However, the efficiency of the beneficiation process can influence the iron content of the tailings. For example, iron ore tailings disposed of in older tailings dams in the Quadrilátero Ferrífero region typically have higher iron content than those generated by current operations (Carneiro et al., 2023). This suggests that tailings that stored at different times within the same facility may exhibit differences in mineralogy and particle shape, impacting the critical friction ratio.

Figure 4.5 illustrates the effect of grading on instability and brittleness index. Five undrained triaxial tests carried out at same mean effective stresses and within a small range of state parameter were selected for this analysis (0.09 to 0.11). Figure 4.5a shows that changes in fines content play a role in the onset instability. As shown in Figure 4.5b and Figure 4.5c, instability occurred at very low axial strain ($\varepsilon_a \approx 1\%$). This behaviour raises concerns about the reliability of displacement meters for monitoring tailings storage facilities. Small strain changes generated large pore pressure responses, bringing the test relatively quickly to the critical state (Jefferies and Been, 2015).

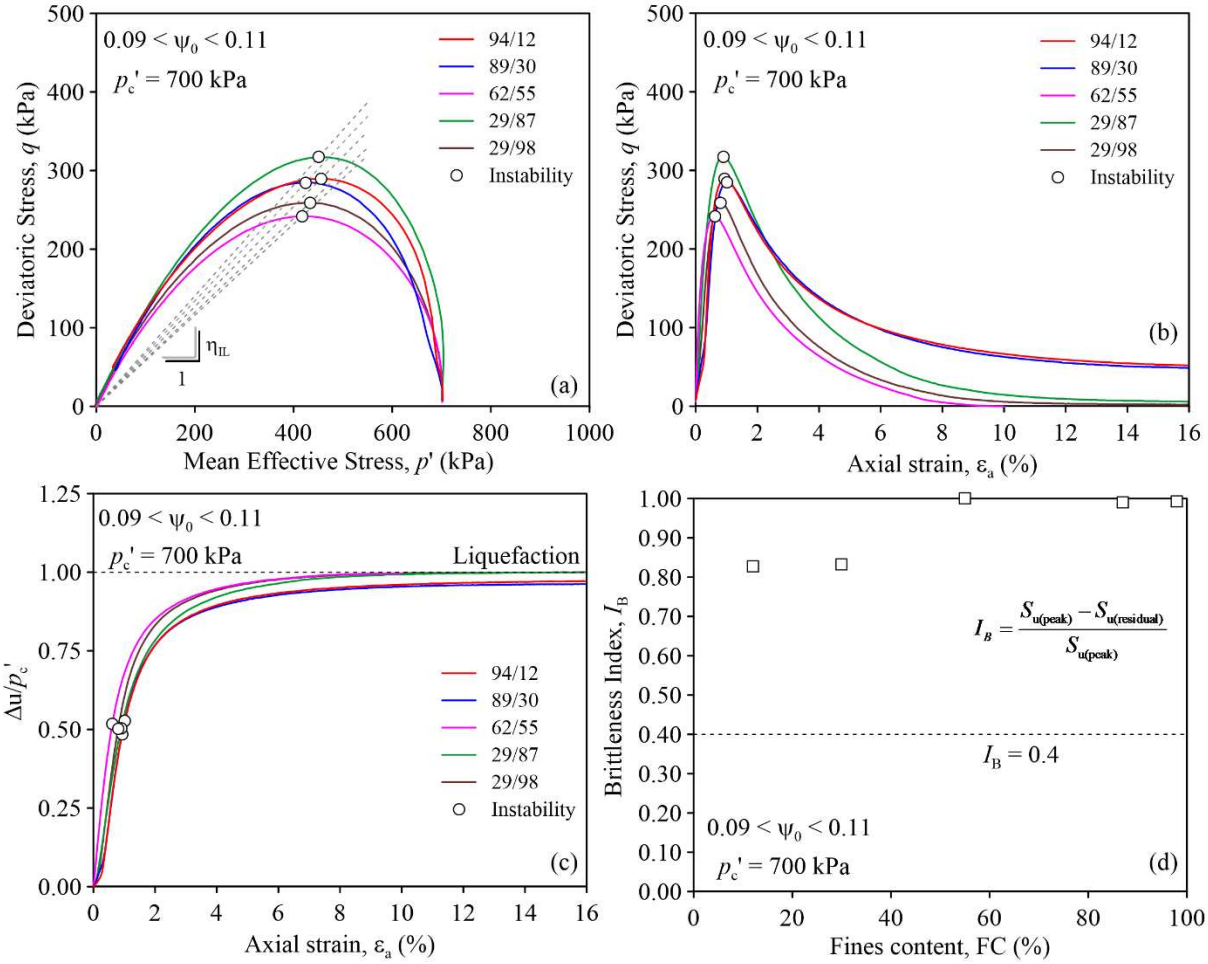

Figure 4.5. Effect of fines content on: (a) instability onset in q-p' plane; (b) stress-strain response; (c) pore pressure generation; (d) brittleness index.

Bishop (1967) introduced I_B to quantify strength loss. When $I_B = 0$ there is no strength loss, whereas $I_B = 1$ suggests that soil has a full-strength loss. Figure 4.5d presents I_B values for different gradings, alongside the threshold ($I_B > 0.4$), associated with flow liquefaction from case histories (Robertson et al., 2017). The results show that the increase of fines content tends to increase of the brittleness index. It is important to highlight that this analysis is specific to a given mean effective stress. Increasing the effective stress may reduce in I_B, as observed by Robertson et al. (2017).

Figure 4.6 illustrates the effect of grading changes on the instability stress ratio, η_{IL} (q_{IL}/p'_{IL}). The green region between dashed lines in Figure 4.6a represents the range of maximum and minimum η_{IL}, values obtained from tested mixtures. The highest value (η_{IL}=0.706) was obtained for the 29/87 mixture (sample collected from the TSF), while the lowest value (η_{IL}=0.580) was observed for the 62/55 mixture; representing a reduction of

approximately 18%. This suggests that in the 62/55 mixture, static liquefaction may be triggered by a smaller effective stress changes during undrained loading, compared to the 29/87 mixture.

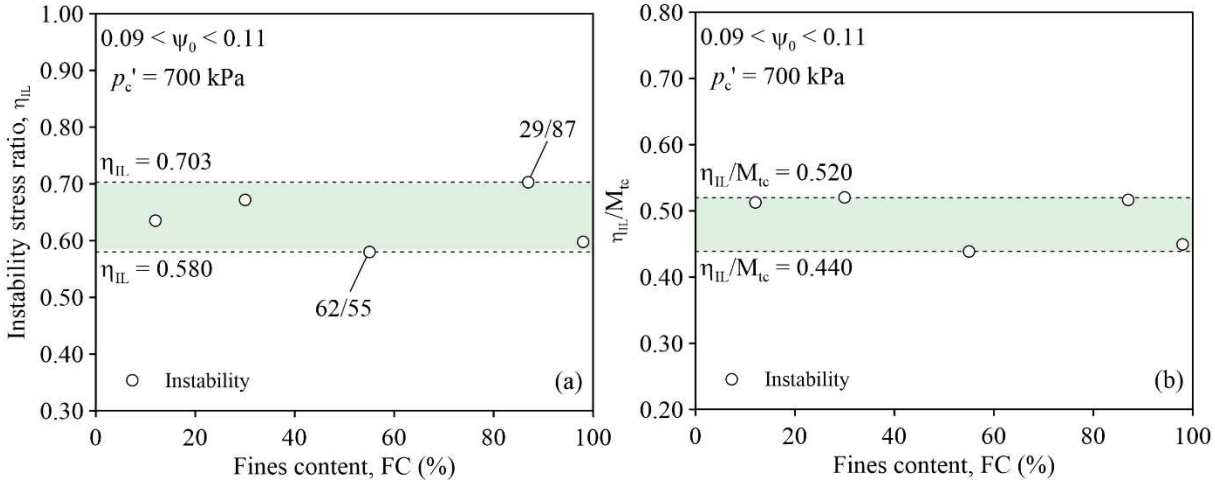

Figure 4.6. Effect of fines content on instability stress ratio.

Fines content was observed to influence both the instability ratio (η_{IL}) and the critical friction ratio (M_{tc}). Figure 4.6b shows the normalized η_{IL}/M_{tc} against fines content. The highest and the lowest values of η_{IL}/M_{tc} were 0.520 and 0.440, respectively, indicating a reduction of approximately 15%. Even after normalizing the instability ratio by the friction ratio, the ratio still varied with the fines content. This suggests that other soil properties must be considered to explain the observed variation. According Jefferies and Been (2015) instability locus is not a soil property but depends on both elastic and plastic properties. Future research that considers these soil properties may contribute to a better understanding of how fines content influences the instability locus.

The analyses of the influence of fines content on the instability locus presented so far refer to loose specimens (e.g., $0.09 < \psi_0 < 0.11$). As the specimens become denser, the state parameter decreases and η_{IL} increases. To illustrate this effect, a series of undrained triaxial compression tests were carried out on the 29/87 mixture, prepared using different molding techniques (air dried and moist tamping), covering a wide range of state parameters. These results were then compared with the soil and mining tailings database compiled by Reid (2020), as shown in Figure 4.7. As expected, η_{IL} increases with decreasing ψ_0. A single instability locus (red dashed line) was inferred, regardless of the specimen preparation method. Comparison with the database compiled by Reid (2020) indicates that the inferred instability locus aligns well with those observed for other materials reported in the literature.

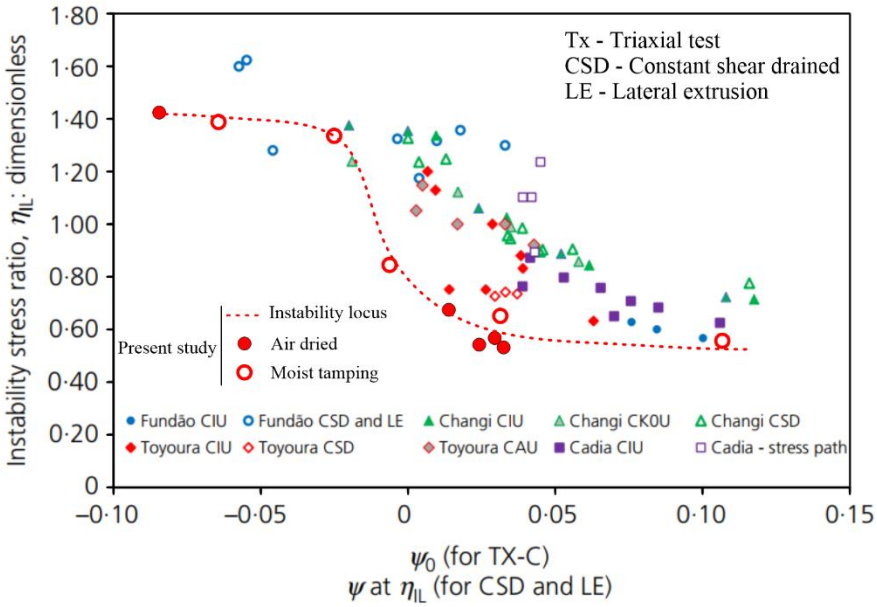

Figure 4.7. Instability stress ratios versus state parameter for the 29/87 mixture and a database compiled by Reid (2020) (adapted from Reid, 2020).

4.2. INFLUENCE OF STRESS PATH ON INSTABILITY LOCUS

The instability locus has been widely studied within the critical state soil mechanics, as the stress ratio at instability (η_{IL}) is often correlated with the state parameter, ψ_0 (e.g., Chu et al., 2003; Jefferies and Been, 2016; Reid, 2020; Fanni et al., 2024). Consequently, measurement of the critical state line (CSL) has become a key input for assessing the liquefaction susceptibility of geomaterials (e.g., Reid et al., 2021a). For this reason, the CSL has been included into the characterization of mining tailings in recent investigations of tailings storage facility failures, including Fundão (Morgenstern et al., 2015), Cadia (Jefferies et al., 2019), and Feijão (Robertson et al., 2019).

Typically, the CSL is defined under triaxial compression loading conditions, assuming that in the e–p′ plane this is independent of density, anisotropy and stress path (Fanni et al., 2025). However, some studies have suggested that CSL in the e-p' plane may depend on Lode angle (θ) or the intermediate principal stress ratio (b) (e.g., Wanatowski and Chu, 2007; Wagner et al., 2023). Given the limited experimental evidence on this topic, further studies are needed to clarify the influence of the magnitude of the intermediate principal stress (σ_2) on the CSL in the *e-p*' plane (Fanni et al., 2025).

Figure 4.8 provides a comparison of the shearing behaviour observed in drained tests carried out on the IOT29/87 mixture using triaxial compression (TXC) and hollow cylinder torsional shear (HCTS) apparatus. The TXC test was performed under a principal stress ratio ($K_c = \sigma_h/\sigma_v$) of 1.0, while the HCTS tests were carried out at $K_c = 0.7$. All specimens were prepared using the moist tamping technique and achieved a loose state after consolidation stage, with a state parameter (ψ_0) of approximately 0.10. Figure 4.8a presents the evolution of deviatoric stress (q) with deviatoric strain (ε_q). The influence of the intermediate principal stress ratio (b) on the stress-strain behaviour can be examined through the TXC_100CID-2 test (dashed black line), HCTS03 (green line), and HCTS04 (blue line). The peak deviatoric stresses observed in the HCTS tests were notably lower than those measured in the triaxial compression. This suggests that triaxial compression ($\alpha = 0^o$ and $b = 0$) provides the highest resistance, when compared to HCTS tests ($\alpha > 0^o$ and $b > 0$) (Yoshimine et al., 1998). Furthermore, results from HCTS03 and HCTS04 indicate that increasing the value of b leads to a reduction in q_{max}. These results are consistent with previous study conducted by Cai et al. (2013). For example, Cai et al. (2013) carried out a series of drained tests on sands using hollow cylinder apparatus. These results showed that the peak of deviatoric stress decreases with increase of α.

Figure 4.8b presents the variation of volumetric strain (ε_v) with increasing deviatoric strains (ε_q). While the triaxial compression (TXC) tests achieved a steady state in terms of volumetric strain, the hollow cylinder tests (HCTS) did not reach this condition. It is observed that when TXC reaches its maximum volumetric strain, around 25%, the volumetric strain in the HCTS tests continues to increase slightly. These observations are consistent with the findings reported by Fanni et al. (2022).

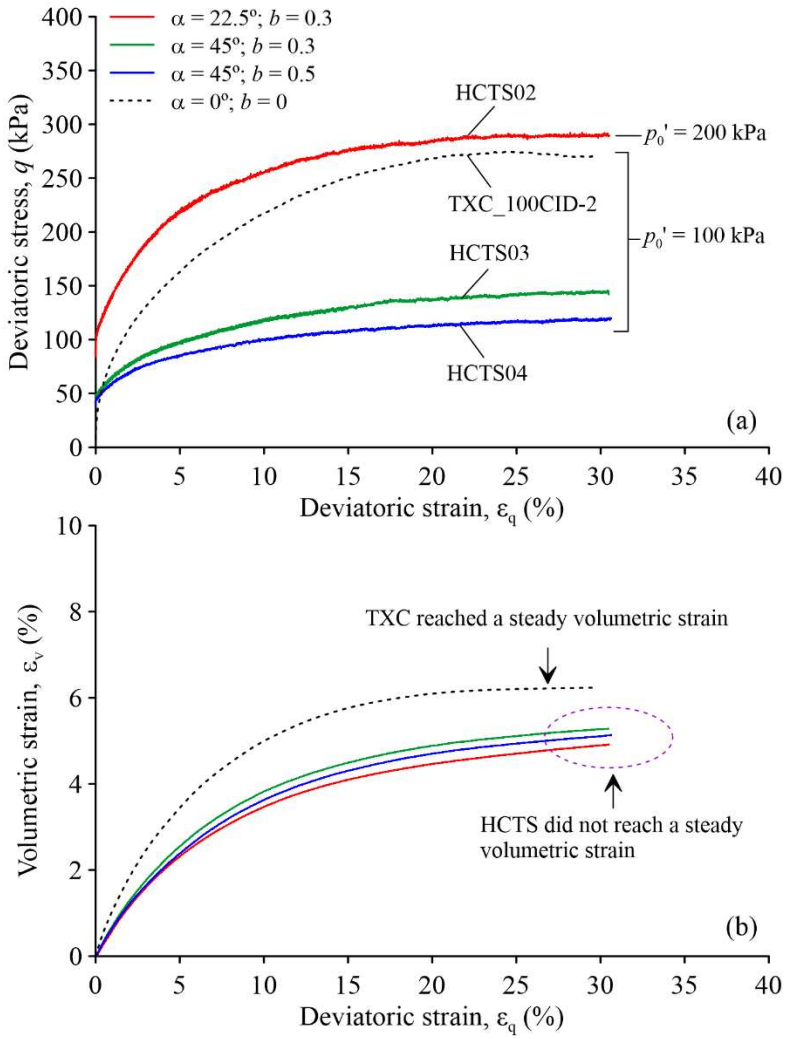

Figure 4.8. Stress–strain behaviour drained tests: (a) q-ε_q plot; (b) ε_v-ε_q plot.

Figure 4.9 is presented to assess the development of the state parameter (ψ) during shearing. The TXC test reaches a near-zero state parameter (ψ = -0.002) at deviatoric strains higher 25%, indicating proximity to the CSL. The HCTS tests also approach the CSL, with ψ values less than 0.01. This small difference is within the range of variability reported in CSL obtained across different laboratories (Reid et al., 2021c), and also within the accuracy of the void ratio measurements in triaxial tests (Nocilla et al., 2006). These findings suggest that, for the studied tailings, the CSL in the e-p′ plane is not dependent on α or *b*. Therefore, the CSL derived from triaxial compression tests may be applied in below-slope plane strain analyses, which are most relevant to perimeter embankment stability (Fanni et al., 2025). This observation is consistent with recent results reported by Fanni et al. (2025).

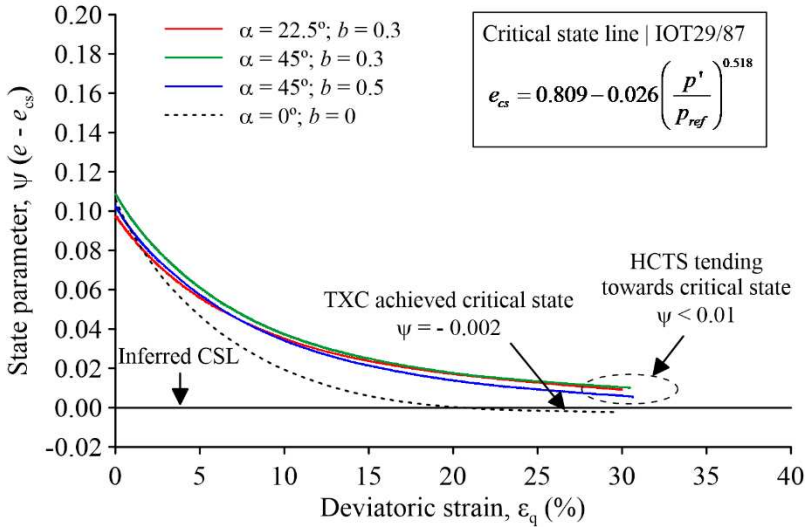

Figure 4.9. Evolution of the state parameter (ψ) during shearing.

Figure 4.10 shows the CSL inferred from triaxial compression tests, in comparison with results from drained hollow cylinder tests. In general, there is good agreement between the points in the critical states obtained from HCTS and those obtained from triaxial compression tests.

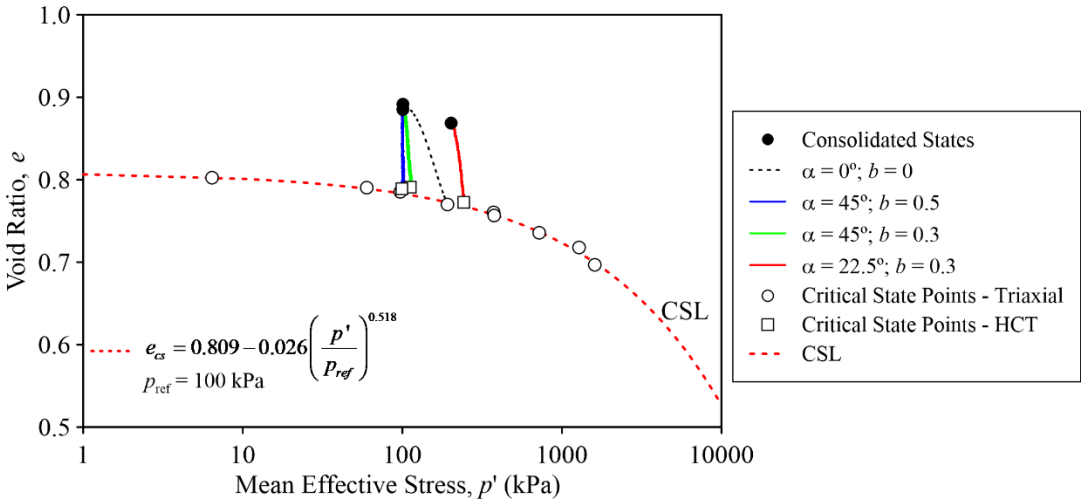

Figure 4.10. Critical state line (CSL) inferred from triaxial compression tests, with comparison to results from drained hollow cylinder tests.

Figure 4.11 shows the critical state line (CSL) inferred from triaxial compression tests, in comparison with results from undrained hollow cylinder tests. All tests were consolidated under $K_c = 0.7$ and $p_c' = 100$ kPa. Arrows indicate the direction of the stress-path at the end of each test. Specimens consolidated above the CSL exhibited contractive behaviour, leading to full liquefaction ($p' = 0$). In contrast, specimens consolidated below the CSL also initially generated positive pore pressure, leading to a reduction in p'. However, during shearing a reversal in

behaviour was observed, resulting in an increase in p' towards the CSL (as indicated by arrows pointing rightward). Although this behaviour is consistent with expectations of critical state soil mechanics (CSSM), these findings reinforce the earlier analysis, suggesting that the CSL in the e-p' plane is not influenced by α or b.

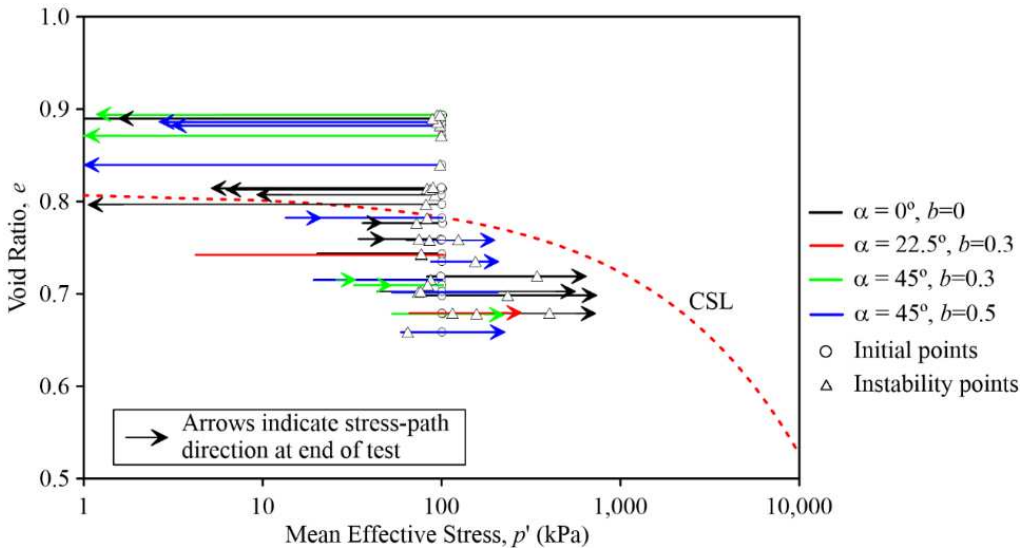

Figure 4.11. Critical state line (CSL) inferred from triaxial compression tests, with comparison to results from undrained hollow cylinder tests.

The corresponding instability lines (η_{IL}) derived from each test are also presented in Figure 4.11. For specimens that exhibited strain-softening behaviour, including those showing QSS (Quasi-steady state) behaviour, η_{IL} was defined at the point of maximum deviatoric stress. In the specimens showing strain-hardening behaviour, instability was considered at the point of maximum η. The criteria adopted in this study to obtain undrained instability were the same as those adopted by Fanni et al. (2024).

The results of the undrained tests carried on MT specimens are illustrated in Figure 4.12. To minimize the influence of density variation on the analysis, specimens with a small range of state parameters (ψ_0) were selected (i.e., ψ_0 between 0.099 to 0.111). The results indicate a slight reduction in η_{IL} with an increase in α, in agreement with the findings reported by Fanni et al. (2024). Furthermore, all specimens exhibited brittle behaviour, reaching instability at very extremely small strains (i.e. in order of 0.1%). This suggests that, within a TSF, even minor perturbation that mobilizes stresses exceeding the instability limit may trigger an immediate strength loss (Been, 2016). The challenges in monitoring mining tailings that exhibit brittle behaviour have led the Global Industry Standard on Tailings Management (GISTM, 2022) to

advise against adopting the full implementation of the observational method for these materials, recommending the adoption of more conservative design criteria.

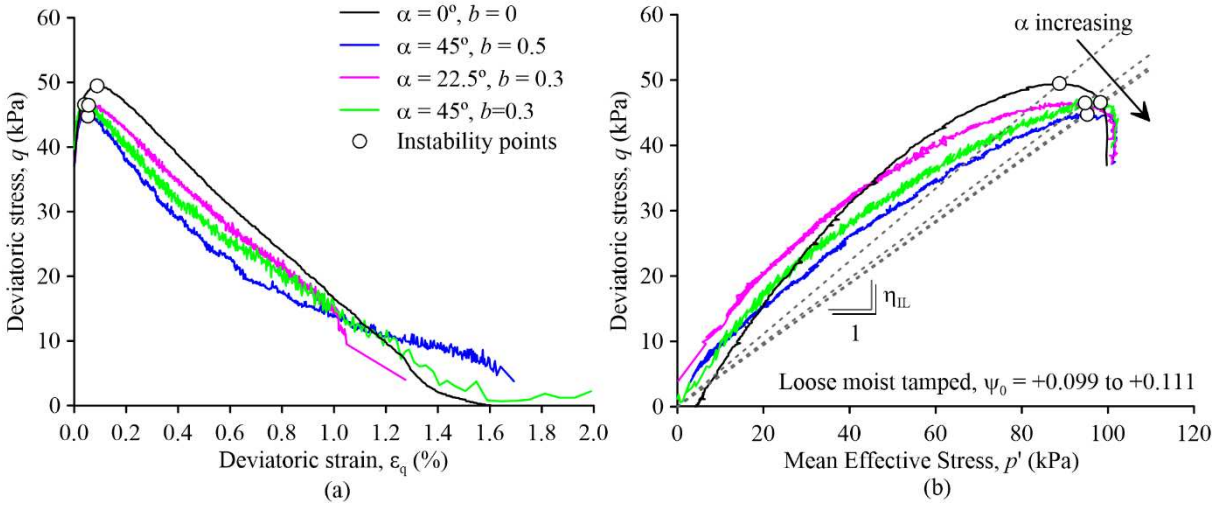

Figure 4.12. Undrained TSHC tests prepared using the moist tamping technique: (a) stress–strain response; (b) q–p′ space.

Figure 4.13 presents the results of undrained triaxial compression and HCTS test performed on moist tamping specimens prepared in medium dense condition ($\psi_0 \sim 0$). Both tests exhibit quasi-steady state (QSS) behaviour, with clear reduction in η_{IL} observed as α increases. QSS behaviour is characterized by a significant post-peak reduction in deviator stress *q*, followed by a minimum strength phase and subsequent dilation towards the CSL (Reid et al., 2023). In the triaxial compression test (α = 0, *b* = 0), η_{IL} was 0.84, whereas in the HCTS test (α = 45º, b = 0.5) a η_{IL} of 0.56 was obtained. These findings are consistent with previous studies evaluating the effect of principal stress angle and intermediate principal stress conditions on QSS behaviour (e.g., Reid et al., 2023; Fanni et al., 2024). The lower peak and post-peak strength observed in the HCTS tests may be attributed to the influence of α and the *b* coefficient on pore pressure development. Yoshimine et al. (1998) reported that increasing the α and b promotes a greater pore pressure generation during shearing.

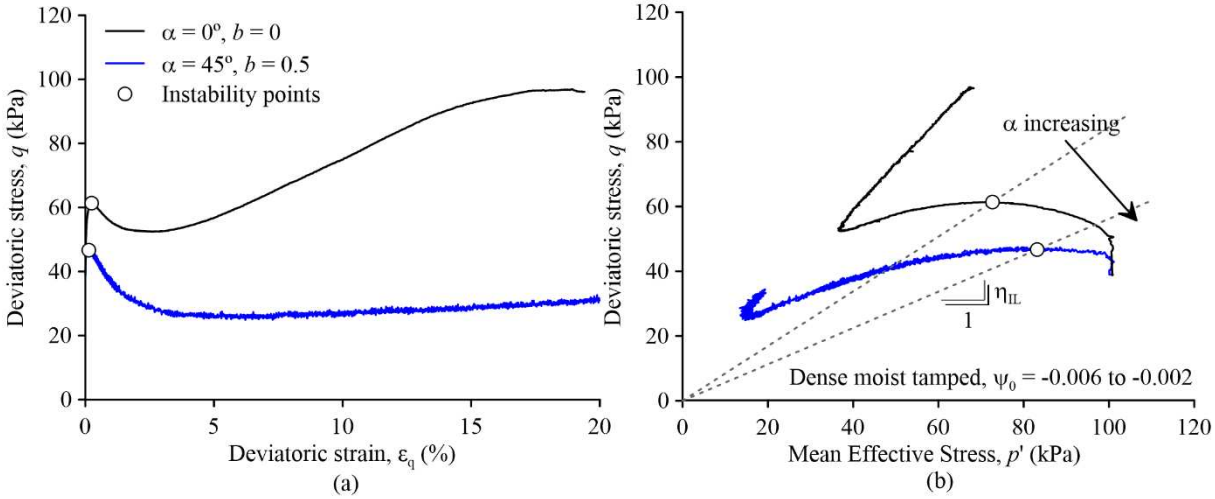

Figure 4.13. (a) Undrained TSHC tests prepared using the moist tamping technique: (a) stress–strain response; (b) q–p′ space.

Figure 4.14 presents the results of undrained triaxial compression and HCTS test carried out on air dried (AD) specimens prepared in dense condition ($\psi_0 \sim$ - 0.075). The specimen tested under triaxial compression condition exhibited dilatant behaviour and high strength, whereas HCTS specimens exhibited QSS behaviour. This comparison highlights the importance of shearing specimens under loading condition that simulate below-slope stress conditions (Reid et al., 2023).

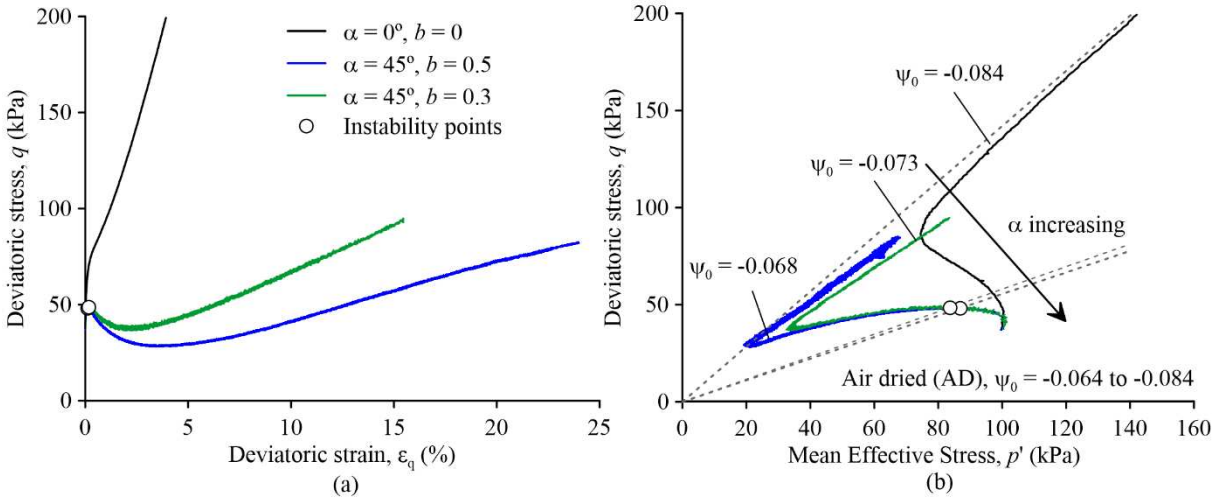

Figure 4.14. Undrained TSHC tests prepared using the air-dried technique: (a) stress–strain response; (b) q–p′ space.

Figure 4.15 presents the results of undrained triaxial compression and HCTS test performed on air dried specimens prepared in very dense condition (i.e., ψ_0 between -0.125 to -0.104). It is observed that all tests in very dense specimens exhibited strain-hardening

behaviour. Under dilative condition, the instability was taken at the point of maximum mobilized η (Fanni et al., 2024). Although all specimens exhibited strain-hardening behaviour, a greater reduction in *p*' was observed during undrained shearing at the highest α value (α = 45º).

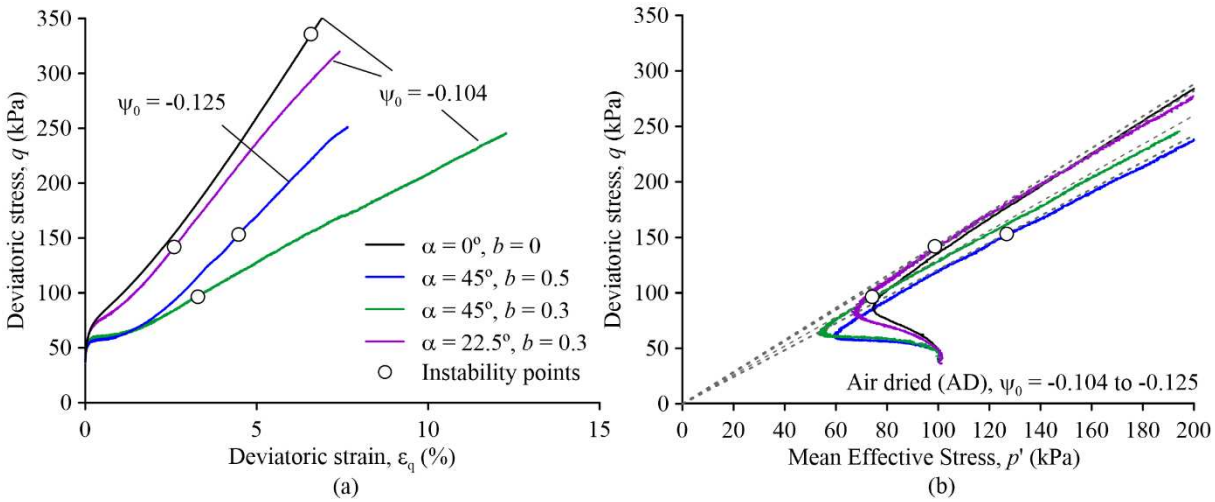

Figure 4.15. Undrained TSHC tests prepared using the air-dried technique: (a) stress–strain response; (b) q–p′ space.

The results presented in Figure 4.13 to 4.15 have important applications for the design and management of tailings storage facilities. The rotation of the principal stresses under below-slope stress conditions may generate a more contractive undrained response. This highlights the need for rigorous compaction control around the perimeter of these tailing storage facilities. Furthermore, Figure 4.14 shows that specimens with ψ_0 slightly less than -0.05 may exhibit strain-softening behaviour, suggesting that the widely used contractive/dilative boundary (Jefferies and Been, 2016), ψ_0 = -0.05, may be unconservative when assessing the static liquefaction susceptibility of below-slope materials.

Figure 4.16 illustrates the effect of increasing α on the normalized η_{IL} (η_{IL}/ η_{IL} at α = 0º), using results from this study and previous tests (Reid, 2020; Reid et al., 2022). Reid (2020) compiled results from HCTS tests performed by Uthayakumar and Vaid (1998), Sivathayalan and Vaid (2002), and Shibuya et al. (2003) on reconstituted sands prepared using the water pluviation technique, whereas Reid et al. (2022) carried out HCTS tests on specimens of undisturbed specimens of gold, copper and platinum tailings. The HCTS results reported by Reid et al. (2022) are identified by gray symbols and their range is highlighted by a yellow

rectangle. It can be observed, in general, that the results obtained in present study are consistent with those reported in the literature, showing a reduction in normalized η_{IL} with increase α.

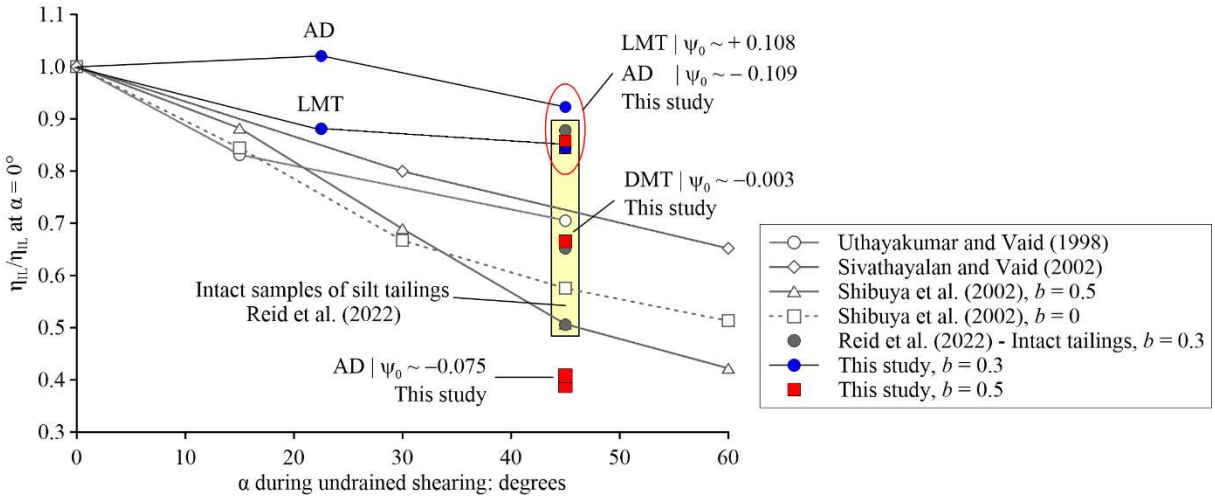

Figure 4.16. Effect of principal stress direction on instability stress ratio from the present study, in comparison with undrained response reported in previous studies (adapted from Reid, 2020 and Reid et al., 2022).

The findings presented in Figure 4.16 also suggest that the state parameter plays a key role in the magnitude of the reduction of η_{IL} with increasing α. Specimens prepared in a very loose state showed a small reduction in η_{IL} (e.g., η_{IL}/η_{IL} at $\alpha = 0^o \sim 0.9$). As the preparation density increased, the influence of the ψ_0 became more pronounced, reaching a maximum reduction at $\psi_0 \sim -0.075$ (e.g., η_{IL}/η_{IL} at $\alpha = 0^o \sim 0.4$). In even denser specimens ($\psi_0 \sim -0.109$), a small reduction in η_{IL} (e.g., η_{IL}/η_{IL} at $\alpha = 0^o \sim 0.9$) was observed, suggesting that for this material, when prepared in either very loose or very dense states, the effect of principal stress direction on undrained shear strength is less pronounced. This indicates that the undrained response varies between the vertical and horizontal planes due to cross-anisotropy effects, and that the magnitude of this effect is state-parameter dependent.

The effect of soil cross-anisotropy on strength has been widely studied over recent decades (i.e., Arthur and Menzies, 1972; Sivathayalan and Vaid, 2002; Lu et al., 2016; Fanni et al., 2024). Recent studies have further highlighted the importance of considering cross-anisotropy in engineering practices involving tailings (i.e., Reid, 2020; Reid et al., 2022; Fanni et al., 2025). Ladd (1991) classified soil anisotropy into three main components: inherent (fabric) anisotropy, initial shear stress anisotropy, and induced (evolving) anisotropy. Inherent anisotropy arises from the soil structure developed at the microlevel (e.g. particle arrangement)

and macrolevel (e.g., layering during deposition) (Ladd, 1991; Fanni et al, 2025. Initial shear stress anisotropy is associated with the one-dimensional strain history and develops when a soil is consolidated under an at-rest consolidation stress (K_0) less than unity (Reid et al., 2022; Fanni et al., 2025). Induced (evolving) anisotropy arises from plastic strains generated by stresses (both consolidation and shear) progressively applied during staged construction (Ladd, 1991).

Induced anisotropy is particularly relevant for the assessment of tailings storage facilities, as it may develop under sloping ground conditions (Fanni et al., 2025). It is important to highlight that both inherent and initial shear stress anisotropies may change due to the effect of induced anisotropy (Fanni et al., 2025). This occurs because applied stresses may alter the inherent soil fabric through particle rearrangement, giving rise to induced fabrics (Yang and Huang, 2023).

In the context of cross-anisotropy, the results presented in Figure 4.16 suggest that the magnitude of the reduction in η_{IL} due to initial shear stress (applying $K_c < 1$) and induced anisotropy (increasing α) may depend on the state parameter. In specimens prepared in a dense state ($\psi_0 \sim -0.075$), the reduction in η_{IL} was much more pronounced compared to other states, suggesting a further induced rearrangement of particles in this condition.

4.3. SHEAR WAVE VELOCITY FOR MONITORING EFFECTIVE STRESS VARIATIONS DURING CSD STRESS PATH

As previously presented and discussed, instability may occur at very low strains, posing additional challenges for monitoring of tailings storage facilities. This issue motivated an investigation into the feasibility of using geophysical methods for monitoring these structures. Five CSD tests were carried out on the IOT87/29 mixture (original tested material) to assess shear wave velocity during the reduction of mean effective stress. Table 4.2 presents the state parameters (ψ_0) reached after consolidation in all CSD tests.

Table 4.2. CSD testing programme: State parameter achieved at end of consolidation

Test ID	Preparation	State	ψ_0
1	MT	Loose	0.095
2	AD	Medium dense	-0.035
3	MT	Loose	0.087
4	AD	Dense	-0.129
5	MT	Loose	0.075

MT is moist tamping; AD is 'air dried'

Figure 4.17 shows stresses and strains developed during the CSD tests, with stress paths plotted in the *q*-*p*' plane for stress paths A, B, and C. Small windows within the figure present the corresponding ε_a-*p*' responses. The figure also includes the critical friction ratio from triaxial tests (M_{tc}) and the onset of instability (η_{IL}) obtained for all tests. The term 'instability' is often used to refer to behaviour where large plastic strain is rapidly generated due to the inability of a soil element to support a given load (Wanatowski et al., 2010). In the present study, the criterion proposed by Chu et al. (2003) was adopted, where the onset of instability is defined as the point at which axial strain acceleration increase rapidly. A similar approach was recently adopted by expert panel that investigated the Cadia failure (Jefferies et al., 2019). Figure 4.17d shows typical strain rate patterns developing in loose and dense specimens and illustrates how the onset instability was identified.

It can be seen from the outcomes presented in Figure 4.17 that the onset of instability occurred prior to reaching the failure state, which is consistent with results reported in previous studies (Wanatowski, 2005; Wanatowski et al., 2010). Arrows indicate the sudden collapse obtained at the end of the tests.

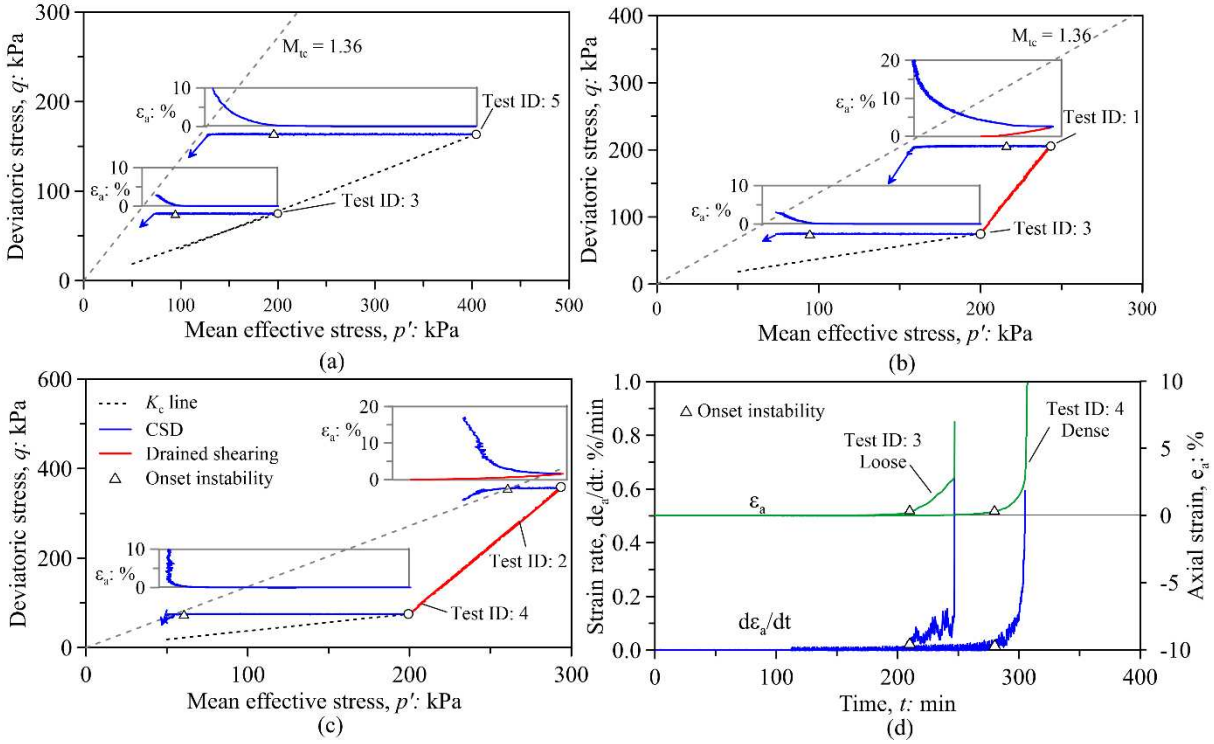

Figure 4.17. (a)-(c) Stress-strain behaviour on CSD tests; (d) typical strain rate patterns developing in loose and dense specimens.

Figure 4.18 presents the CSD results in the *e-p*' plane together with CSL locus. The loose specimens prepared using the moist tamping technique are above the CSL, while the specimens prepared using the air-dried technique are below the CSL. Arrows at the end of the test indicate movement towards the CSL, which is consistent with previous studies (e.g. Wanatowski et al., 2010; Chen and Yang, 2024).

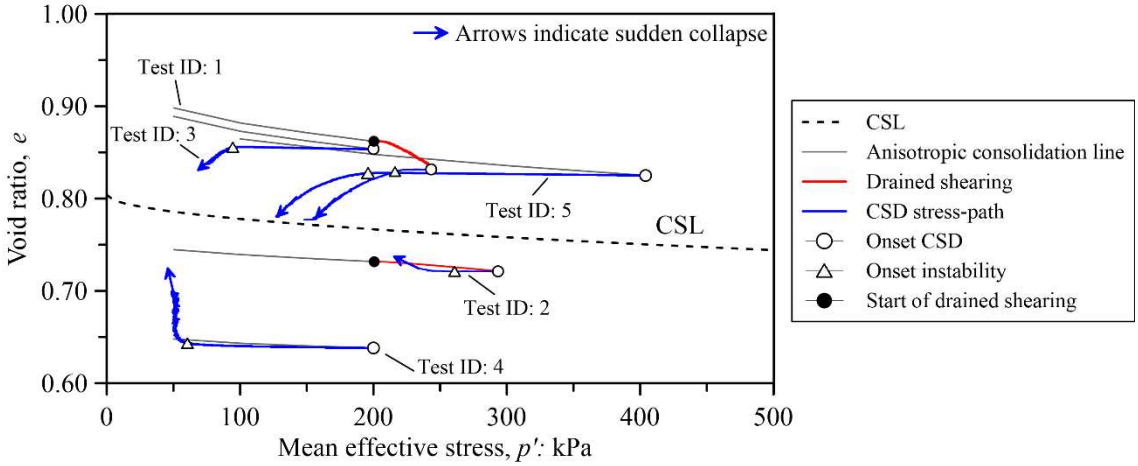

Figure 4.18. Instability behaviour in *e-p*' plane.

Figure 4.19 illustrates the evolution in shear wave velocity measurements during the CSD tests. It also shows the V_s measurement at the end of consolidation stage and their best-fit, expressed as follows:

$$V_s = \alpha\left(\frac{p'}{1\text{kPa}}\right)^{\beta} \quad 3$$

where α is the shear wave velocity at 1 kPa and β is an exponent that captures the sensitivity of V_s to mean effective stress change

In Eq. 3, the stress-dependency exponent β captures both interparticle contact behaviour and fabric changes (Cha et al. 2014). The exponent β was determined for each of five CSD tests by best fitting the shear wave velocity measurement obtained at the end of each consolidation stage. The stress-dependency exponent β obtained in this study ranged from 0.29 to 0.32, which are slightly higher than the typical value of β = 0.25 reported for silica sands (Robertson et al. 1992).

The results presented in Figure 4.19 show a slight increase in V_s during the drained shearing, followed by a decrease in V_s during the CSD stage. It is noted that during the CSD stress path, the V_s measurements continued to follow the same trend as the adjustment derived from the consolidation data (red line). This suggests that shear wave velocity is not strain-dependent and that variations in V_s during the CSD stress path are primarily controlled by changes in mean effective stress. Since V_s is often correlated with elasticity proprieties, such as G_{max}, these findings support the hypothesis adopted in recent elastoplastic models that elasticity is not strain-dependent (Shuttle and Jefferies, 2016; Shuttle et al., 2022).

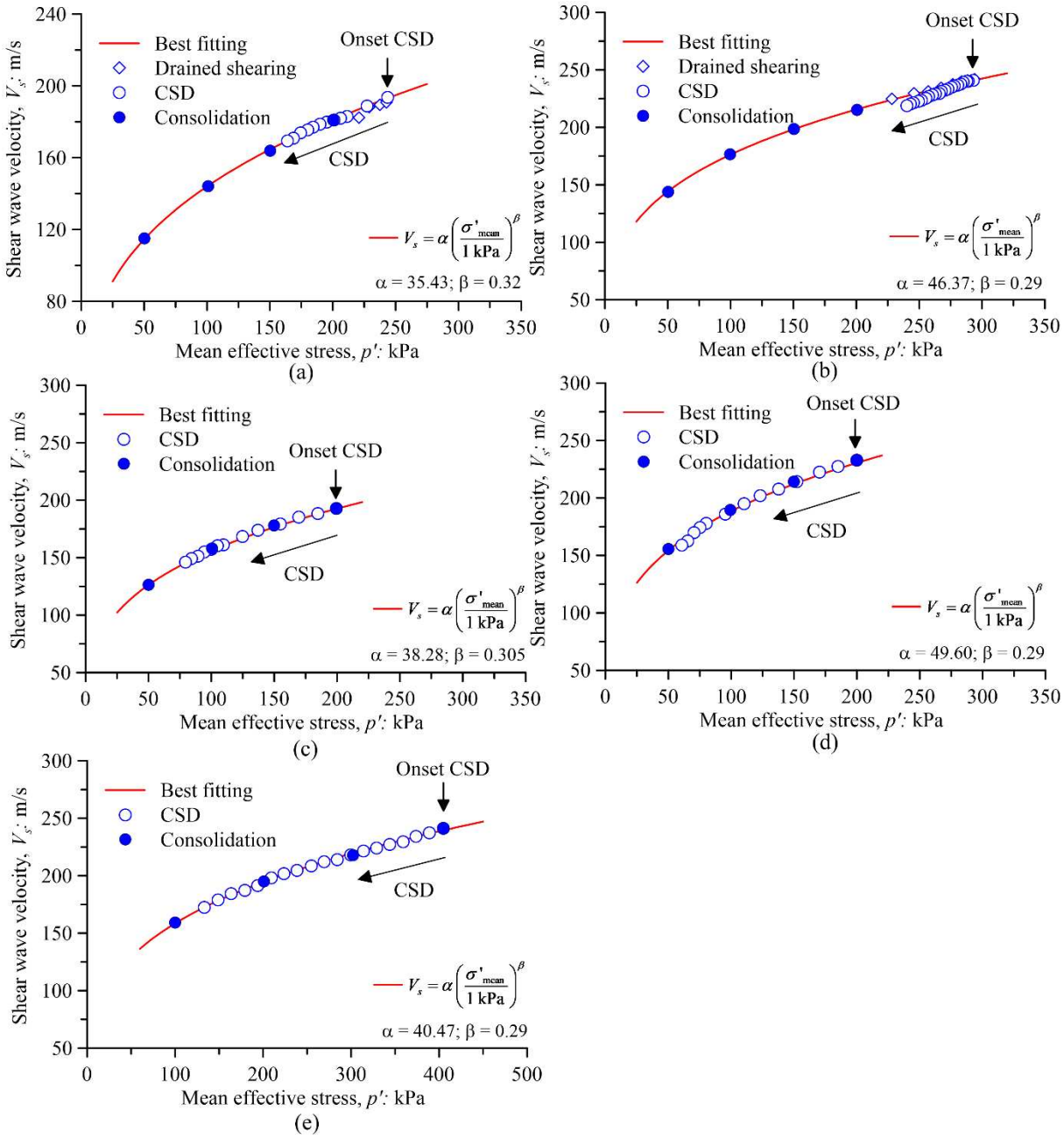

Figure 4.19. Evolution of V_s in all CSD tests: (a) ID: 1; (b) ID: 2; (c) ID: 3; (d) ID: 4; (e) ID: 5.

Figure 4.20 presents the variation in mean effective stress (Δp'), shear wave velocity (ΔV_s) and axial strain ($\Delta \varepsilon_a$) from the onset CSD stage to the onset instability (η_{IL}). For Test ID:5 (i.e., the MT specimen) instability was triggered after a reduction in p' of 193 kPa. During CSD stage, V_s decreased by 43 m/s, whereas ε_a increased by less than 0.5%. This extremely low level of strain mobilization prior to instability highlights the challenge of using surface displacement-based monitoring techniques (e.g. InSAR or ground-based radar). These results are not intended to predict the onset instability or estimate in-situ mean effective stress from V_s

measurements, but rather to suggest that V_s could serve as a useful indicator of reductions in p'.

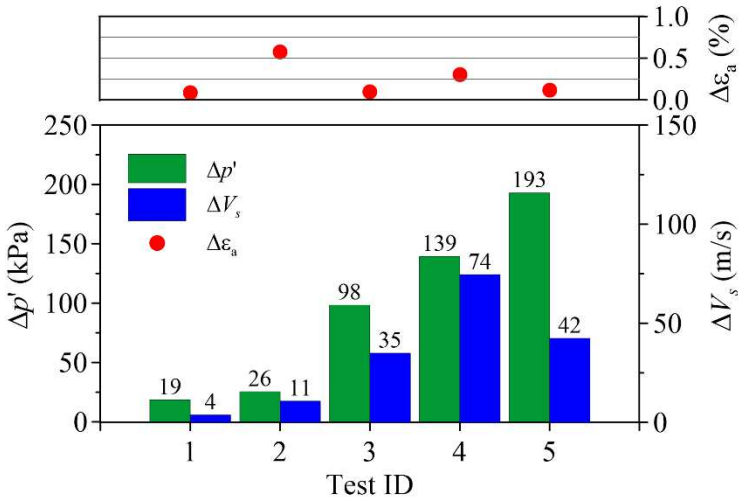

Figure 4.20. Changes in mean effective stress (Δp'), shear wave velocity (ΔV_s), and axial strain ($\Delta \varepsilon_a$) between the onset of CSD and the onset of instability.

4.4. SHEAR WAVE VELOCITY ACROSS A BROAD RANGE OF STATES

The findings presented suggest that V_s measurements may be a valuable tool for monitoring tailings storage facilities. Moreover, several studies have recognized the important role of stiffness evaluation in the triggering of static liquefaction in soils and mine tailings (i.e., Schnaid and Hu, 2007; Schnaid et al., 2013; Riveros and Sadrekarimi, 2020), with G_{max} shown to be a key factor controlling the onset of instability (Jefferies and Been, 2015). While the influence of effective stress and void ratio on sand behaviour is well established (Hardin and Richart, 1963; Hardin and Black, 1966), their effect on stiffness are not yet fully understood for iron ore tailings (Silva et al., 2021). This chapter compiles a database of iron ore tailing, incorporating both available data in the literature and new resonant column tests carried out in this study. The database covers a wide range of void ratios, fines content, specific gravity, and mean effective stress. Figure 4.21 and Table 4.3 illustrate the particle size distribution and the main characteristics for all materials included in this study, respectively.

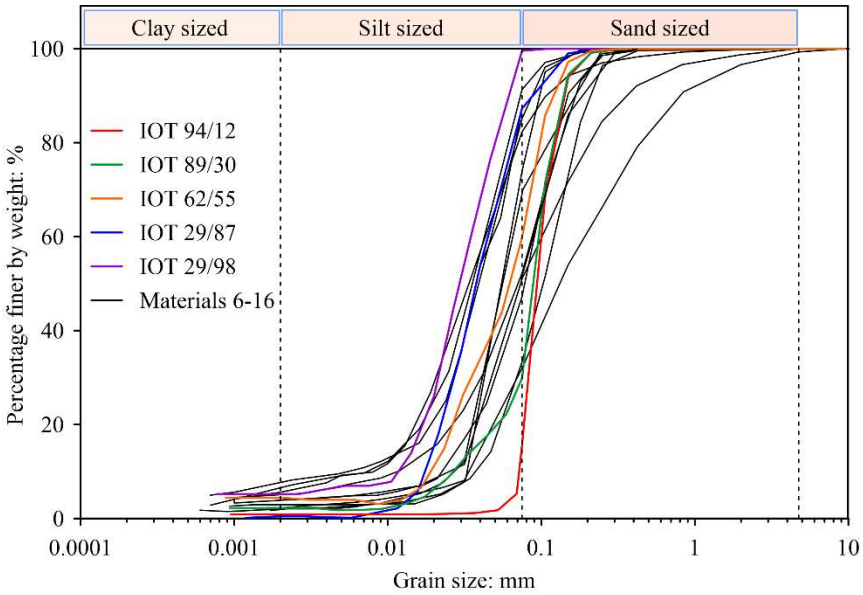

Figure 4.21. Particle size distribution for the materials compiled in this study. Materials IOT 91/12 to IOT 29/98 were produced as part of this study whereas materials 6 to 16 were compiled from Morgenstern et al. (2016), Robertson et al. (2019), Arroyo and Gens (2021), Consoli et al. (2023), Wagner et al. (2023) and Silva et al. (2024).

Table 4.3. Summary of the iron ore tailings database compiled in this study

Material	Γ/λ_e or $e_r/\lambda/\zeta$ (1)	FC	G_s	D_{50} (mm)	Reference
29/87	0.809/0.026/0.518	87	3.36	0.029	This study
94/12	1.132/0.048/0.569	12	2.76	0.094	
29/98	0.869/0.021/0.606	98	3.50	0.029	
89/30	0.993/0.046/0.535	30	2.87	0.089	
62/55	0.793/0.023/0.630	55	3.08	0.062	
06	0.740/0.045/0.460	52	3.05	0.071	Wagner et al. (2023) and Silva et al. (2024)
07	0.860/0.045/0.460	34	2.97	0.103	
08	1.000/0.150/0.245	48	2.83	0.079	Consoli et al. (2024)
09	0.950/0.150/0.232	82	4.02	0.035	
10	1.290/0.340/0.110	71	4.96	0.056	Robertson et al. (2019)(2)
11	1.220/0.340/0.110	51	4.97	0.075	
12	1.190/0.340/0.110	33	4.91	0.132	
13	1.170/0.056	85	3.93	0.039	Arroyo and Gens (2021)(2)
14	1.060/0.051	91	4.54	0.036	
15	1.360/0.050	74	5.00	0.055	
16	0.865/0.024	51	2.80	0.074	Morgenstern et al. (2016)(2)

(1) – Parameters e_r, λ and ζ are the curve fit CSL, whereas Γ and λ_e are the linear approach parameters;

(2) – Materials 10-15 and 16 correspond to the Feijão and Fundão failures, respectively.

The parameters β and α capture the effect of interparticle contact behaviour and fabric changes (Santamarina and Cascante, 1996; Santamarina et al., 2001). Cha et al. (2014) compiled a database covering a wide range of soils, represented by empty symbols in Figure 4.22, and proposed a relationship between α and β. In addition, Figure 4.22 also includes α and β values obtained from data compiled in this study, shown as blue circular symbols. The data for iron ore tailings align well with those published by Cha et al. (2014), and are consistent with results previously reported by Arroyo and Gens (2021) and Silva et al. (2021). This agreement suggests that the α–β trend proposed by Cha et al. (2014) can be reliably extended to iron ore tailings, supporting the broader use of α and β in describing the behaviour of these materials.

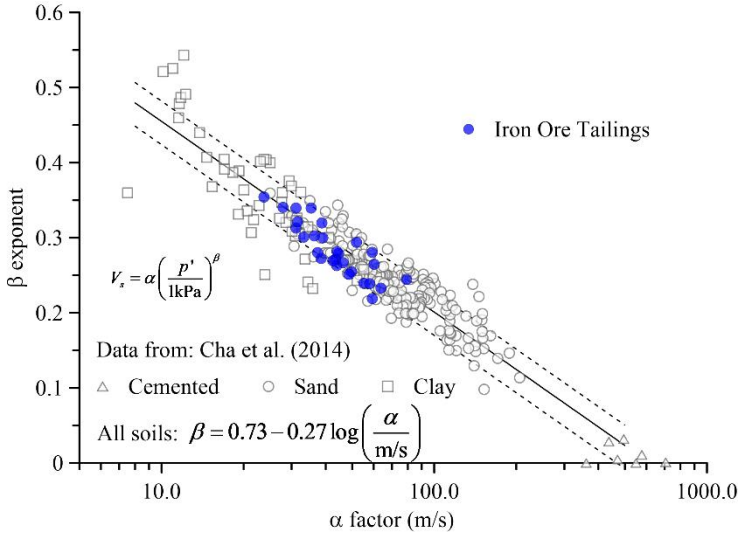

Figure 4.22. Inverse relationship between the β-exponent and the α-factor. The cemented, sand and clay data were obtained from Cha et al. (2014).

Figure 4.23 presents the α and β values obtained for all materials compiled in this study, grouped according to their state parameter (ψ_0) evaluated at a mean effective stress of 100 kPa. A threshold of ψ_0 = - 0.05 was use to classify the results as either dense (ψ_0 < - 0.05) or loose state (ψ_0 > - 0.05). This boundary is supported by laboratory tests and various field-scale analysis of flow liquefaction case histories in sands and silts (Jefferies and Been, 2015). The findings indicate that V_s measurements in dense states exhibits lower stress dependency (i.e., lower β values) compared to loose states, highlighting the influence of state on wave propagation behaviour. In other words, stiffer materials (i.e., those higher V_s) tend to show higher α values but lower β values (Santamarina et al., 2001).

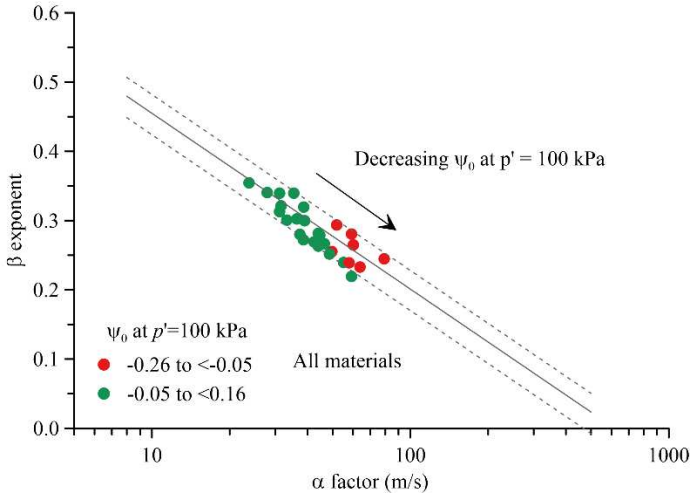

Figure 4.23. Relationship between the β and α for all materials analyzed, grouped according to their state parameter at *p'* of 100 kPa.

In critical state soil mechanics, dense soils tend to exhibit dilative behaviour during shearing, whereas loose tend to show contractive and potentially liquefiable behaviour. Figure 4.24 illustrates how shear wave velocity changes with mean effective stress for all materials compiled in this study, with the data grouped according to their state parameter.

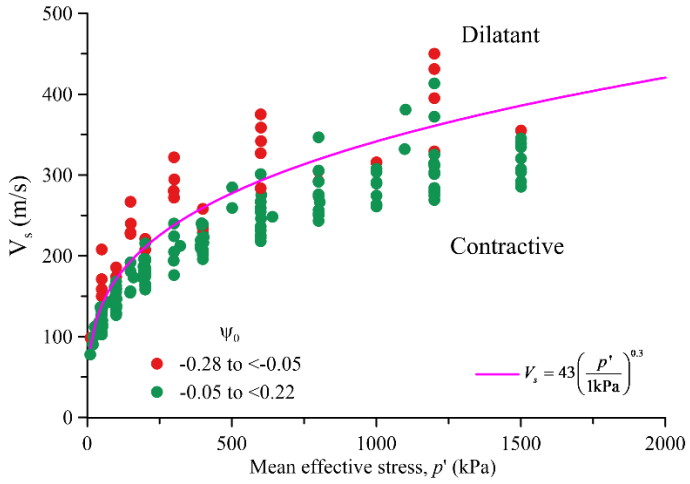

Figure 4.24. Relationship between the β and α for all materials analyzed, grouped according to their state parameter.

A qualitative boundary (indicated by the pink line in the Figure 4.24) was drawn to separate materials exhibiting dilatative behaviour from those showing contractive behaviour. It is important to highlight that this boundary should be used as a qualitative reference only, which can be expressed as follows:

$$V_s = 43\left(\frac{p'}{1\text{kPa}}\right)^{0.3} \qquad 4$$

The influence of factor such as aging and reconstitution techniques on V_s requires further investigation. Complementary studies are being developed to clarify these issues.

CHAPTER 5

5. CONCLUSIONS

This thesis presented an experimental investigation into the instability locus in iron ore tailings, focusing on the influence of material grading and stress path conditions. In addition, the study assessed the applicability of shear wave velocity measurements for monitoring purposes and examined the role of the state parameter in controlling shear wave velocity behaviour. The conclusions drawn from this research are addressed according to the four main objectives, as outlined below:

a) Influence of gradation on the critical state locus and the instability stress ratio

   The experimental results demonstrated that the critical state locus, on both the *e-p*' and *q-p*' planes, is influenced by fines content. This behaviour may be attributed to changes in mineralogy and particle shape introduced by the addition of fines in the mixtures studied. Both the instability stress ratio and the brittleness index were also affected by the gradation, highlighting the importance of considering the particle size distribution effect in the undrained response of iron ore tailings. These findings suggest that fines content is a key factor in assessing the liquefaction triggering of tailings storage facilities. However, the implication of these results for numerical modelling and monitoring practices justifies further investigation.

b) Effect of principal stress rotation (α) and intermediate principal stress ratio (b) under below-slope stress conditions on instability stress ratio

   The drained hollow cylinder tests indicated that the CSL in the *e-p'* plane is not affected by variations in α or b. This finding has practical significance, as it suggests that the CSL *e-p*' obtained from axisymmetric triaxial compression tests may be used to assess tailings behaviour under below-slope stress conditions. Increases in both of α and b lead to a more contractive undrained response compared to standard triaxial compression, resulting in lower instability stress ratios. The magnitude of this effect was found to be dependent of state parameter (ψ_0).

c) Applicability of shear wave velocity for monitoring effective stress variations during CSD paths

Bender elements tests performed during the CSD stress path demonstrated that shear wave velocity is a reliable indicator of changes in mean effective stress in tailings. During the drained shearing, V_s exhibited a slightly increased, whereas in the CSD phase, V_s decreased in response to the reduction in p'. These findings suggest that V_s measurements can capture early changes in effective stress that may not be evident through conventional piezometric or displacement monitoring.

d) Influence of the state parameter on shear wave velocity

The results indicate that Vs measurements in dense states exhibit lower stress dependency compared to loose states. This observation has important implications for tailings management, as it suggests that in very loose deposits, the stiffness of the material is highly sensitive to changes in mean effective stress. Under stress path involving p' reduction (e.g., CSD or lateral extrusion), this behaviour may reflect a significant reduction in stiffness during shearing. Furthermore, a boundary between contractive and dilative response based on shear wave velocity measurements was proposed.

5.1. SUGGESTIONS FOR FUTURE RESEARCH

The following suggestions are proposed for future research:

- Effect of fabric, aging, and cementation: This study was performed using reconstituted specimens under controlled laboratory conditions. Further studies should investigate the influence of in situ fabric, aging, and cementation on the mechanical behaviour of iron ore tailings.
- Cyclic Loading Conditions: The experimental programme focused was limited to monotonic loading conditions. It is recommended that future work examine the response of iron ore tailings under cyclic loading.
- Field-Scale Validation: The present study focused on laboratory testing of reconstituted specimens. Future research should include in situ investigations and testing of undisturbed samples collected from tailings storage facilities.

CHAPTER 6

6. CONCLUSÕES

Esta tese de doutorado apresentou uma investigação experimental sobre a instabilidade em rejeitos de minério de ferro, como foco na influência granulometria do material e das trajetórias de tensões. Além disso, o estudo avaliou a aplicabilidade de medições de velocidade de onda cisalhante para fins de monitoramento de estruturas de armazenamento de rejeitos e examinou o papel do parâmetro de estado no comportamento da velocidade de onda cisalhante. As conclusões obtidas nesta pesquisa são apresentadas de acordo com os quatro principais objetivos, conforme descrito a seguir:

a) Influência da granulometria na linha de estados críticos e na razão de tensões na instabilidade

   Os resultados experimentais demonstram que a linha de estados críticos, tanto nos planos *e-p*' quanto *q-p*', é influenciado pelo teor de finos. Esse comportamento pode ser atribuído a mudanças na mineralogia e na forma das partículas introduzidas pela adição de finos nas misturas estudadas. Tanto a razão de tensões na instabilidade quanto o índice de fragilidade também foram afetados pela granulometria, ressaltando a importância de considerar o efeito da granulometria na resposta não drenada de rejeitos de minério de ferro. Esses resultados sugerem que o teor de finos é fator-chave na avaliação de liquefação em barragens de rejeitos. No entanto, as implicações desses resultados para a modelagem numérica e para as práticas de monitoramento justificam investigações adicionais.

b) Efeito da rotação das tensões principais (α) e da razão de tensões principais intermediárias (*b*) na condição sob taludes sobre a razão de tensões na instabilidade

   Os ensaios drenados realizados em ensaios *hollow cylinder* indicaram que a linha de estados críticos no plano *e-p*' não é afetada por variações de α e *b*. Esse resultado tem relevância prática, pois sugere que a CSL no plano *e-p*' obtida a partir de ensaios triaxiais axisimétricos pode ser utilizada para avaliar o comportamento dos rejeitos em condições de tensões sob taludes. Aumentos em α e b levaram a uma resposta não drenada mais contrátil em comparação ao ensaio triaxial convencional, resultando em

menores razão de tensões na instabilidade. A magnitude desse efeito mostrou ser dependente do parâmetro de estado (ψ_0).

c) Aplicabilidade da velocidade de onda cisalhante para monitoramento de variações de tensões efetivas durante trajetória de tensão do tipo CSD

   Ensaios com *bender elements* realizados ao longo da trajetória de tensão do tipo CSD demonstraram que a velocidade de onda cisalhante é um indicador confiável de mudanças na tensão efetiva média em rejeitos. Durante o cisalhamento drenado, o V_s apresentou ligeiro aumento, enquanto na fase CSD, o V_s diminuiu em resposta à redução de *p*'. Esses resultados sugerem que medições de V_s podem capturar alterações iniciais nas tensões efetivas que podem não ser evidentes em monitoramento convencionais, com piezômetros ou medidores de deslocamento.

d) Influência do parâmetro de estado na velocidade de onda cisalhante

   Os resultados indicaram que as medições de V_s em estados densos apresentaram menor dependência da variação de tensões efetivas, quando comparadas a estados soltos. Essa observação possui implicações relevantes para a gestão de rejeitos, pois sugere que, em depósitos muito soltos, a rigidez do material seria bastante sensível às variações de *p*'. Sob trajetória de tensões que envolvem redução de *p*' (como CSD ou extrusão lateral), esse comportamento pode induzir uma redução significativa da rigidez do material. Além disso, foi apresentado uma fronteira entre a resposta contrátil e dilatante com base em medições de velocidade de onda cisalhante.

REFERENCES

ARROYO, M. & GENS, A. (2021). Computational Analyses of Dam I Failure at the Corrego de Feijao Mine in Brumadinho, Final Report. International Centre for Numerical Methods in Engineering (CIMNE), Technical University of Catalonia, Barcelona, Spain

ARTHUR, J.R.F. & MENZIES, B. K. (1972). Inherent anisotropy in a sand. Géotechnique 22(1): 115–128.

Australian Standard (AS) (2003). Methods of testing soils for engineering purposes—Soil classification tests—Determination of the particle size distribution of a soil—Standard method of fine analysis using a hydrometer (AS 1289.3.6.3).

Australian Standard (AS) (2006). Methods of testing soils for engineering purposes—Soil classification tests—Determination of the soil particle density of a soil—Standard method. (AS 1289.3.5.1).

FOURIE, A.B., & PAPAGEORGIOU, G. (2001). Defining an appropriate steady state line for Merriespruit gold tailings. Canadian Geotechnical Journal, 38(4), 695-706.

Australian Standard (AS), (2009). Methods of testing soils for engineering purposes—Soil classification tests—Determination of the particle size distribution of a soil—Standard method of analysis by sieving (AS 1289.3.6.1)

BEEN, K. (2016). Characterizing mine tailings for geotechnical design. Australian Geomechanics Journal, 51(4): 59-78.

BISHOP, A.W. (1967). Progressive failure – with special reference to the mechanism causing it. Proc. Geotechnical Conf., Oslo, Vol.2:142–150

CARNEIRO, J.J.V., MARQUES, E.A.G., VIANA DA FONSECA, A.J.P., FERRAZ, R.L. & OLIVEIRA, Â.H.C. (2023). Characterization of an iron ore tailing sample and the evaluation of its representativeness. Geotechnical and Geological Engineering, 41(5), 2833-2852.

CARRERA, A., COOP, M. & LANCELLOTTA, R. (2011). Influence of grading on the mechanical behaviour of Stava tailings. Géotechnique, 61(11)

Chen, Y., & Yang, J. (2024). Initiation of flow liquefaction in granular soil slopes: drained versus undrained conditions. Acta Geotech., 19(1): 39–53.https://doi.org/10.1007/s11440-023-01958-6

CHERIF TAIBA, A., MAHMOUDI, Y., BELKHATIR, M., KADRI, A. & SCHANZ, T. (2018). Experimental characterization of the undrained instability and steady state of silty sand soils under monotonic loading conditions. International Journal of Geotechnical Engineering, 12(5): 513–529.

CHO, G.C., DODDS, J. & SANTAMARINA, C.J. (2006). Particle shape effects on packing density, stiffness, and strength: natural and crushed sands. Journal of Geotechnical and Geoenvironmental Engineering, 132(5): 591–602.

CHU, J., LEROUEIL, S. & LEONG, W. K. (2003). Unstable behaviour of sand and its implication for slope instability. Canadian Geotechnical Journal, 40(5): 873-885.

CLARKSON, L. & WILLIAMS, D. (2020). Critical review of tailings dam monitoring best practice. International Journal of Mining, Reclamation and Environment, 34(2): 119-148.

CONSOLI, N.C., SILVA, J.P.S., WAGNER, A.C., CARVALHO, J.V.D.A., BAUDET, B.A., COOP, M.R., SCHEUERMANN FILHO, H.G., CARVALHO, C., SOUSA, G.M. & CACCIARI, P.P. (2024). Critical state analysis of two compacted filtered iron ore tailings with different gradings and mineralogy at different stages of treatment. Acta Geotechnica, 19(2): 881–898.

CUNNING, J. C., ROBERTSON, P. K. & SEGO, D. C. (1995). Shear wave velocity to evaluate in situ state of cohesionless soils. Can. Geotech. J., 32(5): 848–858.

ECKERSLEY, D (1990). Instrumented laboratory flowslides. Géotechnique,40: 489–502. doi:10.1680/geot.1990.40.3.489.

FANNI, R., REID, D. & FOURIE, A. (2022). On reliability of inferring liquefied shear strengths from simple shear testing. Soils and Foundations, 62(3): 101151.

FANNI, R., REID, D. & FOURIE, A. (2023). A simple method to calculate the void ratio of very loose silts and silty sands in torsional shear hollow cylinder testing. Geotechnical Testing Journal, 46(3): 445-465.

FANNI, R., REID, D. & FOURIE, A. (2024). Effect of principal stress direction on the instability of sand under the constant shear drained stress path. Géotechnique, 74(9): 875-891.

FANNI, R., REID, D. & FOURIE, A. (2025). Drained and undrained behaviour of a sandy silt gold tailings under general multiaxial conditions. Géotechnique, 1-67.

FOURIE, A., VERDUGO, R., BJELKEVIK, A., TORRES-CRUZ, L. A. & ZNIDARCIC, D. (2022). Geotechnics of mine tailings: a 2022 state of the art. In Proceedings of "20th International Conference on Soil Mechanics and Geotechnical Engineering.

GISTM Global industry standard on tailings management. (2020). ICMM (International Council on Mining & Metals), UNEP (United Nations Environment Programme) and PRI (Principles for Responsible Investment).

HARDIN, B.O. & BLACK, W.L. (1966). Sand stiffness under various triaxial stresses. J. Soil Mech. Found. Div., ASCE, 92(2): 27–42.

HARDIN, B.O. & RICHART, F.E. (1963). Elastic wave velocities in granular soils. Journal of the Soil Mechanics and Foundations Division 89(1): 33–65.

JEFFERIES, M., MORGENSTERN, N.R., VAN ZYL, D. & WATES, J. (2019). Report on the NTSF embankment failure, Cadia Valley Operations for Ashurst Australia, Document No. H356804-00000-22A-230-0001, pp. 1–119.

JEONG, S. W. & PARK, S.S. (2019). Effect of the surface roughness on the shear strength of granular materials in ring shear tests. Applied Sciences, 9(15), 2977.

LADD, C.C. (1991). Stability evaluation during staged construction. J. Geotech. Engng 117, No. 4, 540–615.

LEONG, E. C., CAHYADI, J. & RAHARDJO, H. (2009). Measuring shear and compression wave velocities of soil using bender–extender elements. Can. Geotech. J., 46(7):792–812

LI, X.S. & WANG., Y. (1998). Linear Representation of Steady-State Line for Sand. Journal of Geotechnical and Geoenvironmental Engineering 124(12): 1215–1217.

LÜ, X., HUANG, M, & ANDRADE, J.E. (2016). Strength criterion for cross-anisotropic sand under general stress conditions. Acta Geotechnica, 11: 1339-1350.

MORGENSTERN, N.R., VICK, S.G., VIOTTI, C.B. AND WATTS, B.D. (2016). Fundão Tailings Dam Review Panel: Report on the Immediate Causes of the Failure of the Fundao Dam. Cleary Gottlieb Steen and Hamilton LLP, New York, NY.

NOCILLA, A., COOP, M. R. & COLLESELLI, F. (2006). The mechanics of an Italian silt: an example of 'transitional'behaviour. Géotechnique, 56(4), 261-271.

RABBI, A.T.M.Z., RAHMAN, M.M. & CAMERON, D. (2019). Critical state study of natural silty sand instability under undrained and constant shear drained path. Int. J. Geomech. 19 (8): 1–13.

REID, D. (2020). On the effect of anisotropy on drained static liquefaction triggering. Géotechnique Letters, 10(3): 393-397.

REID, D., CHIARO, G., FANNI, R. & FOURIE, A. (2022a). Arguments for increasing the use of hollow cylinder testing in the characterization of tailings. In Tailings and Mine Waste.

REID, D., DICKINSON, S., MITAL, U., FANNI, R., & FOURIE, A. (2021a). On some uncertainties related to static liquefaction triggering assessments. Proceedings of the Institution of Civil Engineers-Geotechnical Engineering, 175(2): 181-199.

REID, D., OREA, I., FANNI, R. & FOURIE, A. (2021b). A modular base platen assembly to increase the efficiency of triaxial critical state testing. Proceedings of the 7th International Conference on Tailings Management

REID, D., FANNI, R. & FOURIE, A. (2022b). Effect of tamping conditions on the shear strength of tailings. International Journal of Geomechanics, 22(3), 04021288.

REID, D., FANNI, R. & FOURIE, A. (2023). Why is -0.05 state parameter the boundary between contractive and dilative behaviour. In Proceedings of AusIMM Mine Waste and Tailings 2023. Brisbane, Australia.

REID, D., FOURIE, A., AYALA, J.L., DICKINSON, S., OCHOA-CORNEJO, F., FANNI, R., ... & SUAZO, G. (2021c). Results of a critical state line testing round robin programme. Géotechnique, 71(7): 616-630.

REID, D., FOURIE, A., DICKINSON, S., SHANMUGARAJAH, T., FANNI, R., SMITH, K., ... & DUYVESTYN, A. (2024). Results of a dilatancy round robin. Geotechnical Research, 1-27.

REID, D., SIMMS, P., SIVATHAYALAN, S., FANNI, R. & FOURIE, A. (2022c). The "air dried" specimen reconstitution technique–review, refinements, and applications. In Tailings and Mine Waste.

RIVEROS, G.A. & SADREKARIMI, A. (2020). Static liquefaction behaviour of gold mine tailings. Canadian Geotechnical Journal, 58(6): 889–901.

ROBERTSON, P.K., DE MELO, L., WILLIAMS, D.J. & WILSON, G.W. (2019). Report of the Expert Panel on the Technical Causes of the Failure of Feijão Dam I. Vale S.A., Rio de Janeiro, Brazil.

ROBERTSON, P.K., WOELLER, D.J. & FINN, W.D.L. (1992). Seismic cone penetration test for evaluating liquefaction potential under cyclic loading. Can. Geotech. J., 29(4): 686–695.

SANTAMARINA, C. & CASCANTE, G. (1996). Stress anisotropy and wave propagation: a micromechanical view. Canadian Geotechnical Journal, 33(5): 770–782.

SANTAMARINA, J.C., KLEIN, K.A. & FAM, M.A. (2001). Soils and Waves: Particulate Materials Behavior, Characterization and Process Monitoring. Wiley, Chichester.

SCHNAID, F. & YU, H.S. (2007). Theoretical interpretation of the seismic cone test in granular soils. Géotechnique, 57(3):265–272

SCHNAID, F., BEDIN, J., VIANA DA FONSECA, A.J.P., & DE MOURA COSTA FILHO, L. (2013). Stiffness and strength governing the static liquefaction of tailings. Journal of Geotechnical and Geoenvironmental Engineering, 139(12): 2136–2144.

SHIBUYA, S., HIGHT, D. W. & JARDINE, R. J. (2003). Four-dimensional local boundary surfaces of an isotropically consolidated loose sand. Soils Found. 43(2):89–103.

SHUTTLE, D. & JEFFERIES, M. (2016). Determining silt state from CPTu. Geotech. Res., 3(3): 90–118.

SHUTTLE, D., MARINELLI, F., BRASILE, S. & JEFFERIES, M. (2022). Validation of computational liquefaction for tailings: Tar Island slump. Geotech. Res., 9(1): 32–55.

SILVA, J.P.S., CACCIARI, P.P., RIBEIRO, L.F. & JEFFERIES, M. (2022). Influence of compaction on small-strain shear modulus of iron ore tailings. Proceedings of the Institution of Civil Engineers-Geotechnical Engineering, 175(2), 247-260.

SILVA, J.P.S., CARVALHO, J.V., WAGNER, A.C. & CONSOLI, N.C. (2024). On the behavior of compacted filtered iron ore tailings submitted to high pressures. In E3S Web of Conferences, 544, p.13004. EDP Sciences.

SIVATHAYALAN, S. & VAID, Y.P. (2002). Influence of generalized initial state and principal stress rotation on the undrained response of sands. Can. Geotech. J. 39, No. 1, 63–76

THEVANAYAGAM, S., SHENTHAN, T., MOHAN, S. & LIANG, J. (2002). Undrained fragility of clean sands, silty sands, and sandy silts. Journal of Geotechnical and Geoenvironmental Engineering, 128(10): 849–859.

TORRES-CRUZ, L.A. & SANTAMARINA, J.C. (2020). The critical state line of nonplastic tailings. Canadian Geotechnical Journal, 57(10): 1508-1517.

UTHAYAKUMAR, M. & VAID, Y.P. (1998). Static liquefaction of sands under multiaxial loading. Can. Geotech. J. (35)2: 273–283.

Viana da Fonseca, A., Ferreira, C. & Fahey, M. (2009). A framework interpreting bender element tests, combining time-domain and frequency-domain methods. Geotech. Test. J., 32(2): 91–107.

Viana da Fonseca, A.V., Cordeiro, D. & Molina-Gómez, F. (2021). Recommended procedures to assess critical state locus from triaxial tests in cohesionless remoulded samples. Geotechnics, 1(1): 95-127.

Vulpe, C. (2024). Upgrading a resonant column apparatus to reliably measure specimen void ratio. In Proceedings of the 7th International Conference on Geotechnical and Geophysical Site Characterization. International Centre for Numerical Methods in Engineering (CIMNE).

Wagner, A.C., de Sousa Silva, J.P., de Azambuja Carvalho, J.V., Rissoli, A.L.C., Cacciari, P.P., Chaves, H.M., et al. (2023). Mechanical behavior of iron ore tailings under standard compression and extension triaxial stress paths. Journal of Rock Mechanics and Geotechnical Engineering, 15(7): 1883–1894.

Wanatowski, D. & Chu, J. (2007). Static liquefaction of sand in plane strain. Canadian Geotechnical Journal 44: 299–313.

Wanatowski, D., Chu, J. & Loke, W.L. (2010). Drained instability of sand in plane strain. Canadian Geotechnical Journal 47: 400–412

Yang, S., & Huang, D. (2023). Investigating the influence of inherent soil fabrics on reliquefaction resistance of sands using DEM-clump simulation. Computers and Geotechnics, 164: 105817.

Yoshimine, M., Ishihara, K., & Vargas, W. (1998). Effects of principal stress direction and intermediate principal stress on undrained shear behavior of sand. Soils and foundations, 38(3): 179-188.